AGU PUBLICATIONS

Water Resources Research

RESEARCH ARTICLE
10.1002/2015WR017660

Companion to
Hale and McDonnell [2016],
doi:10.1002/2014WR016124.

Key Points:
- Distinct subsurface storage zones with unique water ages identified
- Dynamic mixture of storage zones sets stream water mean transit time
- Subsurface permeability contrasts dictate storage zone discretization

Correspondence to:
V. C. Hale,
chale@nutterinc.com

Citation:
Hale, V. C., J. J. McDonnell, M. K. Stewart, D. K. Solomon, J. Doolitte, G. G. Ice, and R. T. Pack (2016), Effect of bedrock permeability on stream base flow mean transit time scaling relationships: 2. Process study of storage and release, *Water Resour. Res.*, *52*, 1375–1397, doi:10.1002/2015WR017660.

Received 15 JUN 2015
Accepted 6 JAN 2016
Accepted article online 2 FEB 2016
Published online 28 FEB 2016

Effect of bedrock permeability on stream base flow mean transit time scaling relationships: 2. Process study of storage and release

V. Cody Hale[1], Jeffrey J. McDonnell[2,3], Michael K. Stewart[4], D. Kip Solomon[5], Jim Doolitte[6], George G. Ice[7], and Robert T. Pack[8]

[1]Nutter and Associates, Inc., Athens, Georgia, USA, [2]Global Institute for Water Security, National Hydrology Research Centre, University of Saskatchewan, Saskatoon, Saskatchewan, Canada, [3]Northern Rivers Institute, School of Geosciences, University of Aberdeen, Aberdeen, UK, [4]Aquifer Dynamics and GNS Science, Lower Hutt, New Zealand, [5]Department of Geology and Geophysics, University of Utah, Salt Lake City, Utah, USA, [6]USDA Natural Resources Conservation Service, Harrisburg, Pennsylvania, USA, [7]National Council for Air and Stream Improvement, Inc., Corvallis, Oregon, USA, [8]Civil and Environmental Engineering, Utah State University, Logan, Utah, USA

Abstract In Part 1 of this two-part series, Hale and McDonnell (2016) showed that bedrock permeability controlled base flow mean transit times (MTTs) and MTT scaling relations across two different catchment geologies in western Oregon. This paper presents a process-based investigation of storage and release in the more permeable catchments to explain the longer MTTs and (catchment) area-dependent scaling. Our field-based study includes hydrometric, MTT, and groundwater dating to better understand the role of subsurface catchment storage in setting base flow MTTs. We show that base flow MTTs were controlled by a mixture of water from discrete storage zones: (1) soil, (2) shallow hillslope bedrock, (3) deep hillslope bedrock, (4) surficial alluvial plain, and (5) suballuvial bedrock. We hypothesize that the relative contributions from each component change with catchment area. Our results indicate that the positive MTT-area scaling relationship observed in Part 1 is a result of older, longer flow path water from the suballuvial zone becoming a larger proportion of streamflow in a downstream direction (i.e., with increasing catchment area). Our work suggests that the subsurface permeability structure represents the most basic control on how subsurface water is stored and therefore is perhaps the best direct predictor of base flow MTT (i.e., better than previously derived morphometric-based predictors). Our discrete storage zone concept is a process explanation for the observed scaling behavior of Hale and McDonnell (2016), thereby linking patterns and processes at scales from 0.1 to 100 km^2.

1. Introduction

In Part 1 of this two-part series, *Hale and McDonnell* [2016] showed that bedrock permeability controlled stream base flow mean transit time (MTT) and MTT scaling relationships for two nested, mesoscale catchments in western Oregon, USA. Despite striking similarities in hydrologic regime, topography, soil hydraulic properties, and vegetation, MTTs and MTT scaling relationships were distinctly different between the two catchments. The defining difference between the catchments was the permeability of the bedrock—one deeply weathered and fractured marine-derived sandstones and siltstones (Drift Creek-Oregon Coast Range; eight nested subcatchments included in this study) and the other with poorly permeable volcanic bedrock (primarily massive breccias and tuffs) with fractures only significant within the top 3 m (HJ Andrews (HJA)—Western Cascades Range; seven nested subcatchments). The sandstone catchments had distinctly longer MTTs (mean MTT was 6.2 years, $n = 8$) than the volcanic catchments located less than 140 km to the west (mean MTT was 1.8 years, $n = 7$). More importantly, the scaling relationships that allow MTT to be estimated based on easily attainable catchment characteristics were different; MTTs at the more permeable sandstone catchments (Drift Creek) scaled best with catchment area while MTTs at the volcanic catchments (HJA) were highly correlated to indices of catchment topography (flow path gradient and length) and showed no correlation with catchment area.

The MTT scaling relationships at the HJA, originally reported by *McGuire et al.* [2005], have been linked mechanistically to shallow, lateral subsurface flow initiated by the abrupt permeability contrast at the soil-bedrock interface being the dominant runoff generation process [*Harr*, 1977; *McGuire and McDonnell*,

2010]. In addition to topographic metrics, other studies have shown that MTT scales with other factors, including soil type and drainage class [*Soulsby et al*., 2006; *Tetzlaff et al*., 2014], catchment aspect [*Broxton et al*., 2009], depth of hydrologically active soil and bedrock [*Asano and Uchida*, 2012], or some combination [*Heidbüchel et al*., 2013; *Hrachowitz et al*., 2009; *Rodgers et al*., 2005]. Based on their results and the existing process understanding at the HJA, *Hale and McDonnell* [2016] concluded that the primary control on the different MTT scaling relations they observed was the contrasting subsurface permeability distribution resulting from the specific lithology, structure, and weathering history of the bedrock. However, the specific processes responsible for the MTT behavior of the Drift Creek catchments remain unclear. In fact, given that no other MTT-focused studies to date conducted in small to mesoscale catchments have observed scaling relations where MTT increases with increasing drainage area [*Tetzlaff et al*., 2009], the reasons for such behavior generally are still wanting.

In spite of well-established theory relating the amount of water stored in a catchment to stream discharge [*Botter et al*., 2009; *Brutsaert and Nieber*, 1977; *Kirchner*, 2009; *Rinaldo et al*., 2015], process understanding of subsurface water storage generally remains a poorly understood component of catchment hydrology [*McNamara et al*., 2011]. It is well recognized that subsurface storage properties play a key role in driving runoff dynamics [*Ali et al*., 2011; *Frisbee et al*., 2011; *Kosugi et al*., 2006; *Oswald et al*., 2011; *Spence*, 2010] and setting stream water geochemical composition [*Anderson et al*., 1997a; *Birkel et al*., 2011b; *Haria and Shand*, 2004; *Manning et al*., 2013; *Rademacher et al*., 2005; *Soulsby et al*., 2007] by regulating where and how fast water flows through the catchment system. Hence, the ability to predict hydrological and/or water quality response to catchment disturbances (e.g., toxic releases, land-cover change, climate change) is predicated on having a solid process understanding of how water is stored and moves through the subsurface [*Kirchner et al*. 2000].

In early conceptualizations of subsurface runoff generation processes [e.g., *Hewlett and Hibbert*, 1967; *Weyman*, 1973; *Whipkey*, 1965], storage was generally considered to be limited to the soil pore space as the underlying bedrock was assumed impermeable (see *Bonell* [1993] for review). However, over the past two decades, researchers have provided unequivocal evidence linking deeper (relative to the soil profile) storage components to runoff generation in steep mountainous catchments (including *Anderson et al*. [1997b], *Asano et al*. [2002], *Blumstock et al*. [2015], *Duvert et al*. [2016], *Frisbee et al*. [2011], *Haria and Shand* [2004], *Kosugi et al*. [2006, 2011], *Millares et al*. [2009], *Rademacher et al*. [2005], *Soulsby et al*. [2007], and *Wilson and Dietrich* [1987]). These storage components can lead to very long residence times of water in the subsurface both during and between events and can skew our understanding of streamflow sources, flow paths, and transit times [*Maloszewski et al*., 1983; *Stewart and Thomas*, 2008; *Stewart et al*., 2007, 2010, 2012; *Uhlenbrook et al*., 2002]. Yet subsurface storage is an inherently difficult characteristic to study because it is largely unobservable with current technology [*Soulsby et al*., 2009]. Notwithstanding recent advancements in ground-based geophysics [*Robinson et al*., 2008] and gravity remote sensing [*Reager and Famiglietti*, 2009], the total storage volume of a catchment is virtually unknowable because the overall control volume is difficult to define. Even when the control volume is reasonably assumed, the internal pore volume and pore connectivity are still poorly characterized by current measurement technologies [*Rinaldo et al*., 2011]. Although recent estimates of storage have been attempted by extrapolating point-based measurements [*McNamara et al*., 2011] and via catchment-based mass balance [*Sayama et al*., 2011], one of the best proxies for characterizing catchment storage is stream water MTT [*Birkel et al*., 2011a; *Fenicia et al*., 2010; *Katsuyama et al*., 2010; *Uchida et al*., 2006].

Mean transit time is defined as the time it takes, on average, for a parcel of water to travel through a catchment from the point of entry to the point of exit [*Bolin and Rodhe*, 1973]. When the steady state assumption of reservoir theory used in lumped-parameter transit time models is applied, MTT is equivalent to turnover time—defined as mobile catchment storage divided by discharge [*Bolin and Rodhe*, 1973]. This important link allows storage to be estimated when stream discharge and MTT are known [*Soulsby et al*., 2009]. We note that the steady state assumptions required for this relationship to hold are never met in catchment studies and that recent theoretical advances now provide the framework for determining time-variant MTT with high temporal resolution tracer data sets [*Benettin et al*., 2013; *Botter et al*., 2012; *Harman*, 2015; *Hrachowitz et al*., 2013, 2010; *Heidbüchel et al*., 2013]. Nonetheless, this methodology provides for the best possible tracer-based approximation of total storage at the catchment scale given current theory and real-world sampling limitations.

So how might catchment storage control MTT ranges and scaling? *Sayama and McDonnell* [2009] showed the effect of catchment storage volume on MTT ranges using a modeling experiment where the

topography, soils, and climate of two well-studied catchments (HJ Andrews WS10 (Oregon, USA) and Maimai M8 (New Zealand)) were interchanged to investigate their influence on stream water MTT. They found that greater soil depth, and hence greater storage, led to longer transit times regardless of which topographic configuration or climate type was used. However, in catchments with complex subsurface features such as fractured bedrock, the relationship between storage and MTT is not as straight forward [*Rinaldo et al*., 2011]. In situations where multiple discrete bedrock aquifers actively and independently contribute to streamflow—as has been observed in Japan [*Kosugi et al*., 2011] and Wales [*Haria and Shand*, 2004]—stream water MTT will be the integration of the unique transit time distribution of each storage component [*Harman*, 2015]. Therefore, the age and relative contribution of each storage component contributing to streamflow sets the stream water MTT [*Botter et al*., 2010]. Further, if the relative contribution of the individual storage components to streamflow changes with storage volume, then stream water MTT will vary as catchment storage varies, as shown by *Niemi* [1978], *Morgenstern et al*. [2010], *Heidbüchel et al*. [2012], and *Soulsby et al*. [2011, 2015]. To date, no empirical studies that we are aware of have assessed the role of catchment storage on the scaling relationships of stream water MTT in small to mesoscale catchments.

Here we use a mechanistic assessment of catchment storage within the Drift Creek catchment in Oregon, USA, employing both water balance methods and MTT-based estimates of storage volumes, to explain the MTT scaling relations of *Hale and McDonnell* [2016]. Water balance storage estimations, referred to as "dynamic storage," are determined by the fluxes of water into and out of the catchment over a given period of time [*Sayama et al*., 2011]. Since MTT-based estimates of storage reference the subsurface volume that the tracer mixes with, including dynamic, mobile water stores, and "passive" (partially immobile, see *Birkel et al*. [2011a]) water stores, it is referred to as "total storage" (this approximation of total storage ignores storage components that are irrelevant to streamflow). To attempt to avoid MTT-based storage estimates that are biased by the MTT truncation reported by *Stewart et al*. [2010], we use ^{3}H-based MTT estimates together with our deuterium-based MTT estimates from *Hale and McDonnell* [2016] to estimate total storage (we note that, as *Frisbee et al*. [2013] show, it is possible for the true transit time distribution of streams in mountainous headwater catchments to include transit times that are longer than what can be captured even by the ^{3}H-based MTT method—this topic is addressed further in section 5.1).

Using ultralow level tritium (^{3}H) measurement capabilities [*Morgenstern and Taylor*, 2009] and a well-characterized ^{3}H input function for our study region (B. Michel, personal communication, 2011), we are able to report, for the first time in the Northern Hemisphere, ^{3}H-based MTT estimates from single stream water samples. In addition, we use a network of shallow and deep bedrock groundwater wells to interrogate and attempt to delineate different subsurface storage zones within the catchment. We use ^{3}H/^{3}He groundwater dating to help develop our conceptual model of how subsurface storage controls stream water MTTs. Although groundwater dating has been proven to be an invaluable tool for understanding groundwater systems [e.g., *Aeschbach-Hertig et al*., 1998; *Cook et al*., 2005, 1996; *Manning and Caine*, 2007; *Manning et al*., 2012], it has sparsely been used in concert with stream base flow MTT studies to reconcile how storage is related to MTT in small to mesoscale catchments [e.g., *Rademacher et al*., 2005; *Duvert et al*., 2016].

We combine our MTT-based storage analyses and ^{3}H/^{3}He groundwater dating with water balance-based storage estimates, borehole characterizations, and groundwater dynamics to investigate the process link between bedrock permeability and MTT scaling relationships. We frame our study around the following questions:

- How does bedrock permeability affect catchment-scale water storage?
- How old is the water in storage?
- What is the process link between MTT scaling and bedrock storage and release?

Lastly, we relate these findings to the intercomparison with the HJ Andrews catchment detailed in *Hale and McDonnell* [2015] to form an overall conceptualization of how bedrock permeability controls subsurface storage, MTTs, and MTT scaling relationships.

2. Study Site

We use the Needle Branch catchment located in the Drift Creek drainage of the Alsea River in the central Coast Range of Oregon (Figure 1; 44.5°N 123.9°W) to investigate the role of catchment storage in controlling MTTs. Needle Branch lies within a highly dissected mountainous area, characterized by short, steep slopes

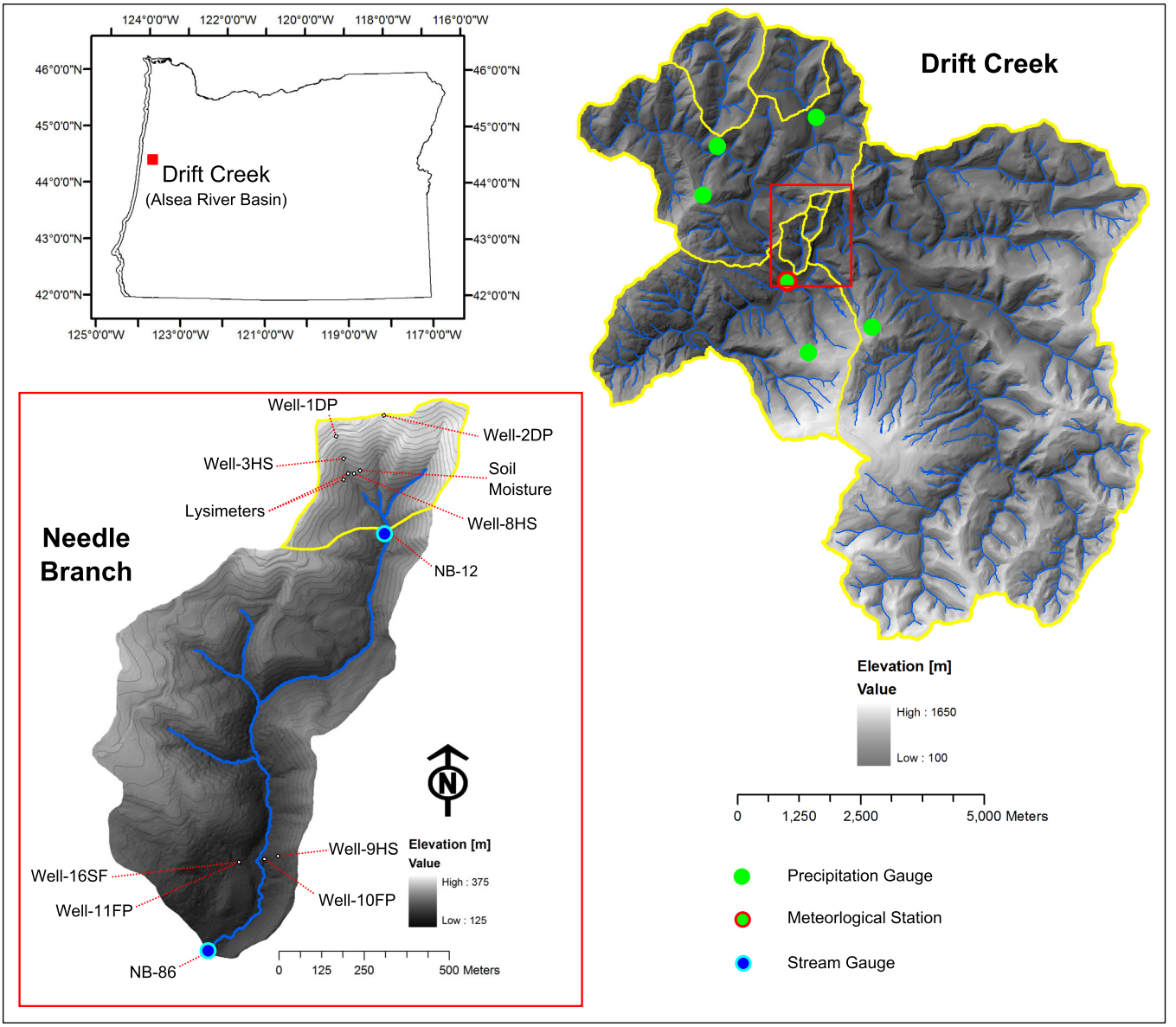

Figure 1. Study site map. Contour intervals are 10 m.

which give rise to medium-gradient to high-gradient streams [*Thorson et al.*, 2003]. Overall topographic relief is 237 m, with an outlet elevation 132 m (NAVD88) and median slope of 34% (see *Hale and McDonnell* [2016] for additional terrain characterization). The catchment is forested with an even-age stand (approximately 40 year old) dominated by Douglas-fir (*Pseudotsuga menziesii*) with red alder (*Alnus rubra*), occurring predominantly along the riparian corridor and occasionally on the hillslopes. Mean annual precipitation for Needle Branch is 2235 mm (PRISM 1971–2000 "normals" grid, PRISM Climate Group, Oregon State University, http://prism.oregonstate.edu, created 16 June 2006). On average, greater than 85% of the annual precipitation occurs from October to April in "long-duration, low-to-moderate intensity frontal storms" [*Harr*, 1976]. Snow accumulation occurs occasionally, but is typically highly transient.

The bedrock underlying the research catchment is the Eocene-aged Tyee Formation comprised by rhythmic-bedded layers of marine-derived greywacke sandstones and siltstones [*Snavely et al.*, 1964]. Boring logs from a series of wells installed throughout the Needle Branch catchment show that the shallow bedrock is weathered and fractured at least to a depth of 9 m below the ground's surface (see *Hale and McDonnell* [2015] for detailed core descriptions). Boring logs from two deep wells installed near the ridge of

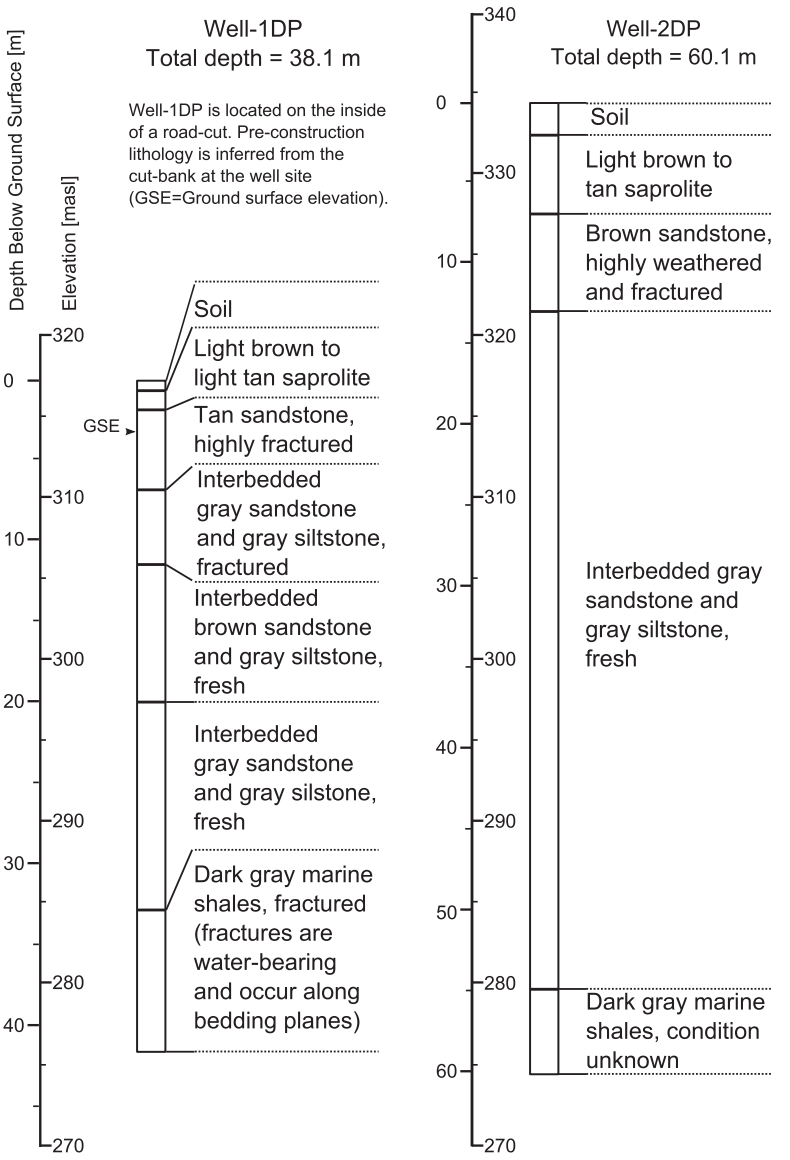

Figure 2. Boring logs from Well-1DP and Well-2DP.

the upper catchment provide further evidence that the highly weathered and fractured zone extends to approximately 10–13 m depth (Figure 2). Well-1DP (DP = deep) was located at the inside of a road-cut; based on the exposed cut section, we estimate that approximately 1.5 m of saprolite and 2 m of fractured bedrock was removed from the location during road installation. Beds of fresh sandstone and siltstones begin at 11.5 m and continue to the installation depth (38.1 m) at Well-1DP. Water-bearing fractures were encountered between 30 and 35 m. Reconnaissance with a downhole camera indicated that these fractures were oriented parallel to the bedding plane and were the only water-bearing fractures observable within the borehole. Approximately 6 m of saprolite and 6 m of highly weathered and fractured rock overlay bedded layers of fresh sandstone and siltstone at Well-2DP (Figure 2). No water-bearing fractures were encountered during the drilling process at Well-2DP, nor were any observable with the downhole camera. The average bed thickness for both boreholes was in agreement with values reported by *Snavely et al.* [1964] for this formation (0.9–1.5 m). Cores were not obtained due to the drilling method employed (based on funding constraints), so detailed information on fracture density with depth is not available. However, a detailed description of a 35 m core drilled at the same landscape position and within the same geologic formation at the Mettman Ridge experimental hillslope was reported by *Anderson et al.* [1997b]. At Mettman

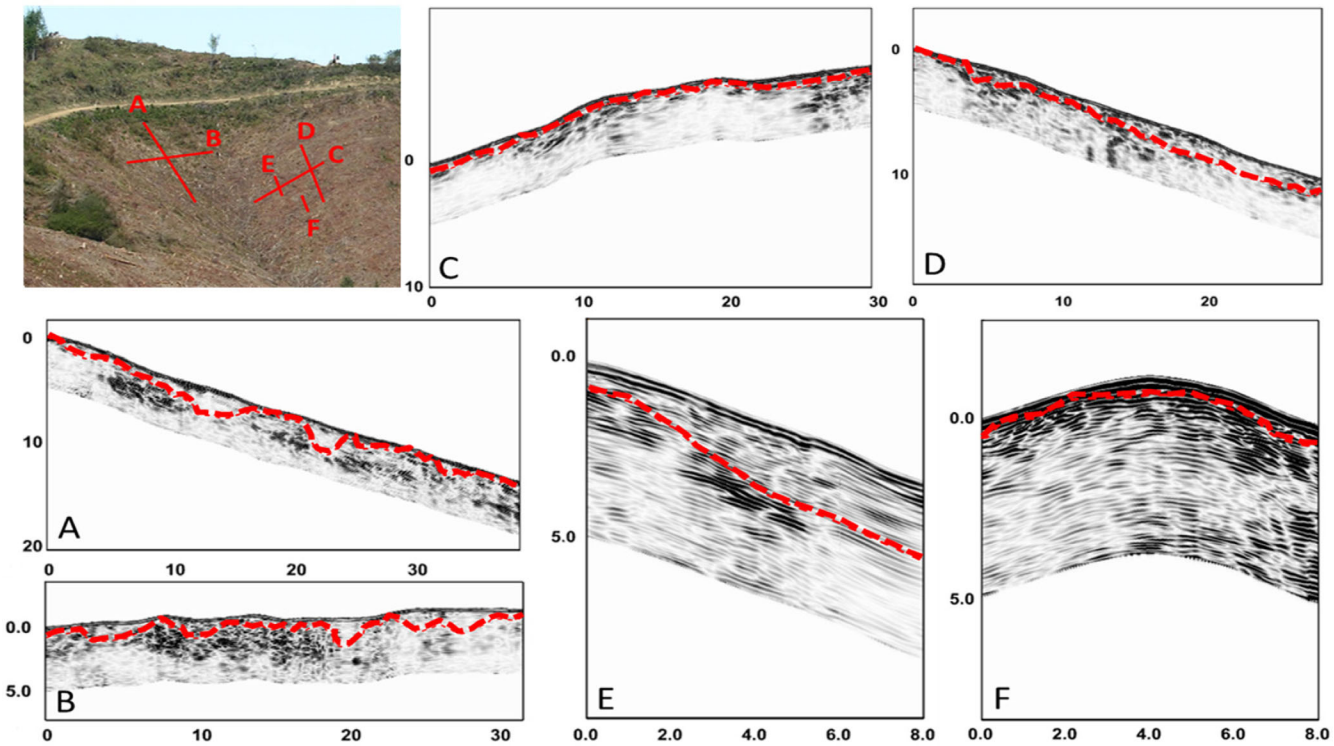

Figure 3. Ground-penetrating radar reflection profiles for transects in the western-most subcatchment of NB-12, A-F, as depicted in the inset photo. Approximate soil-bedrock interface shown as a dashed red line (as interpolated based on differences in reflectivity).

Ridge, approximately 4 m of weathered rock was present directly below 0.5 m of colluvium. Fractured rock, approximately 4 m in thickness and having abundant oxidation features indicating water flow, was encountered below the weathered rock layer. Rock found below the fractured layer was characterized as fresh, although some fractures were present. Oxidized fractures were only present to 24 m of the 35 m borehole. Although this description matches well with the limited data extracted during drilling and camera reconnaissance at the two well installations in Needle Branch, the bedrock does not conform to this "neat" layer-cake structure across the entire catchment. Detailed topographic data obtained through airborne laser altimetry suggest several large areas of subdued topography that was likely created by deep-seated landslides—the presence of which has been documented to increase at this latitude within the Tyee Formation [*Roering et al*., 2005].

Upland soils within the Needle Branch catchment are loams to gravelly loams (mesic Alic Hapludands and mesic Andic Humudepts) that average 1 m depth and are classified as well to very well drained [*Corliss*, 1973]. A ground-penetrating radar survey of two hillslopes in the upper Needle Branch catchment shows that although the soils are generally thin, soil depths can vary significantly over small distances (Figure 3). Field measurements of saturated hydraulic conductivity at the Needle Branch experimental catchment were not possible in most hillslope locations using a constant-head permeameter [*Amoozegar*, 1989] due to extremely high conductivities (that exceed field permeametry limits of $\sim$1000 mm h^{-1}). *Torres et al*. [1998] experienced the same problem using a Guelph Permeameter at Mettman Ridge. Hillslope soils at Mettman Ridge are the same mapped soil series as those in Needle Branch; therefore, soil hydraulic properties measured at Mettman Ridge are assumed to be representative of those within Needle Branch. At Mettman Ridge, *Montgomery et al*. [1997] estimated average saturated conductivities of 10^{-3} m s^{-1} in colluvial soil and 10^{-5} m s^{-1} in the saprolite material forming the C-horizon using falling head tests in a series of piezometers ($n = 28$ for soil and $n = 3$ for saprolite) and found those to be consistent with measurements reported for Oregon Coast Range soils by *Harr* [1977], *Yee and Harr* [1977], and *Hammermeister et al*. [1982]. Also at Mettman Ridge, *Anderson et al*. [1997b] reported porosities averaging 70% ($n = 12$) and *Torres et al*. [1998] showed that these soils have very steep soil water retention curves—meaning that although they transmit water rapidly when at or near saturation, their hydraulic conductivity declines significantly with decreasing

water potential and they retain little water relative to their total porosity. Valley bottom soils in Needle Branch are silt loams (isomesic Fluvaquentic Humaquepts), that average 2 m depth and are classified as moderately permeable and somewhat poorly drained [*Corliss*, 1973].

3. Methods

3.1. Hydrometric Measurements

Stream discharge was measured at two locations in the Needle Branch catchment, NB-12 and NB-86 (number corresponds to catchment area in hectares; locations are marked on Figure 1). The period of record used in the analysis was October 2007 to September 2009 for NB-12 and October 2005 to September 2009 for NB-86 (NB-12 was not installed until October 2007). Precipitation inputs for NB-12 and NB-86 were taken as the areal average of a spatially distributed network of rain gauges located within the vicinity of the Needle Branch catchment (Figure 1).

Soil water content (θ_v) was measured at a profile representing average hillslope soil conditions (i.e., located midslope on a hillslope with average slope, slope length, and soil depth for the catchment; location shown in Figure 1). We installed sensors (Model 10HS, Decagon Devices, Inc., Pullman, WA) at 0.15, 0.30, 0.65, and 0.85 m depths which were chosen to represent dominant textural classes present within the profile. The 0.15 and 0.30 m depths corresponded to upper and lower portions of a gravelly loam A-horizon. The 0.65 m depth was the midpoint in the gravelly, clay loam B-horizon and the 0.85 m depth represented the sandy clay loam BC horizon. Profile water content was estimated on hourly time steps by integrating θ_v for each sensor over its representative depth (0–0.225, 0.225–0.45, 0.45–0.75, and 0.75–1.00 m).

A network of groundwater wells was installed in the Needle Branch catchment. Two deep wells, Well-1DP and Well-2DP, are located approximately 150 m from each other near the ridge forming the northern boundary of the catchment (see Figure 1 for locations and Figure 2 for boring logs). Both DP wells were sealed into fresh rock with steel casing, backfilled with bentonite, and completed as 0.15 m diameter open boreholes. Three hillslope wells were installed into shallow bedrock in Needle Branch using the portable drilling system described by *Gabrielli and McDonnell* [2011]; Well-3HS (HS = hillslope) and Well-8HS are located in the upper catchment (Figure 1) and Well-9HS is located in the lower catchment. The HS wells are all constructed of 25.4 mm inside-diameter (ID) polyvinylchloride (PVC). A 101.6 mm ID PVC outer casing was installed to the depth of the saprolite-bedrock transition. The inner casings were custom-made for each well so that the screened interval was sealed to a depth of 0.5–1 m below the saprolite-bedrock transition. The screen section was created using approximately 0.5 mm horizontal slots; the slotted section was covered with two layers of fiberglass mesh screen to prevent fine particles from entering the well. The annulus between the inner casing and the borehole wall was not large enough to allow backfilling with sand to an accurate, evenly packed depth, so the seal was created by positioning a rubber gasket on the outside of the inner casing such that it fit snugly against the walls of the borehole at the desired sealing depth. Bentonite was backfilled on top of the gasket to the top of the outer casing to finalize the seal (approximately 0.1 m above the ground surface). Two floodplain (FP) wells, Well-10FP and Well-11FP, were installed in the lower Needle Branch catchment (Figure 1). The FP wells were constructed in the same manner as the HS wells and were sealed into the weathered bedrock underlying the surficial alluvial aquifer. Together, Well-9HS, Well-10FP, and Well-11FP are located on a transect perpendicular to the valley axis in lower Needle Branch. Water levels in all wells were measured on 10 min intervals (Model U20, Onset Computer Corporation, Inc., Pocasset, MA).

3.2. Soil Water Mean Transit Time Estimation

Soil water MTT was estimated using the lumped-parameter convolution integral approach [*Maloszewski and Zuber*, 1982] (by definition, the age distribution of water sampled from the catchment subsurface is properly referred to as the residence time distribution with its first moment being the mean residence time, but throughout this paper we refer to this characteristic as soil water mean transit time (MTT) as an attempt to limit confusion by remaining consistent with the terminology used for stream water). The input characterization and modeling procedure employed is described in detail by *Hale and McDonnell* [2016]. The tracer output for the transit time model was characterized by measuring the deuterium composition of soil water (0.5 m depth) collected from two suction lysimeters installed at midslope and toeslope positions in NB-12 near Well-8HS (Figure 1). Samples were collected on daily to weekly intervals from June 2008 to June 2009.

Following *McGuire and McDonnell* [2010] who successfully modeled soil water MTT in similar soils, we used the dispersion flow model [*Maloszewski and Zuber*, 1982] to estimate the transit time distribution, $g(\tau)$, of soil water. The dispersion model is expressed as,

$$g(\tau)=\left(\frac{4\pi D_p\tau}{\tau_m}\right)^{-\frac{1}{2}}\tau^{-1}\ \exp\left[-\left(1-\frac{\tau}{\tau_m}\right)^2\left(\frac{\tau_m}{4\pi D_p\tau}\right)\right], \tag{1}$$

where, D_p is the dispersion parameter (1/Peclet number) and τ_m is the MTT.

3.3. ^{3}H-Based Stream Base Flow MTT Estimation

The lumped-parameter convolution approach employed by *Hale and McDonnell* [2016] to estimate deuterium-based MTTs was used to calculate ^{3}H-based MTTs, except that a radioactive decay term was included in the calculation, so that,

$$C_{out}(t)=\int_0^\infty g(\tau)C_{in}(t-\tau)\,e^{-\lambda\tau}d\tau, \tag{2}$$

where $C_{out}(t)$ is the ^{3}H concentration in streamflow at time t, $g(\tau)$ is the transit time distribution, C_{in} is the precipitation ^{3}H concentration, and $e^{-\lambda\tau}$ is the radioactive decay term (with decay constant $\lambda=\ln(2/T_{1/2})$ and $T_{1/2}=12.32$ years for ^{3}H). We modeled C_{out} based on weighted annual C_{in} using the weighting function,

$$C_{in}=\sum_{i=1}^{12}C_iR_i\Big/\sum R_i, \tag{3}$$

where C_i is the ^{3}H concentration in precipitation and R_i is the recharge amount for month i. We estimated R_i as the difference between monthly precipitation and monthly evapotranspiration. Monthly precipitation ^{3}H measured in Portland, Oregon (B. Michel, unpublished report, 2011), was used for C_i. Where necessary, C_i data gaps were filled using correlations with monthly measurements from Vienna, Austria (International Atomic Energy Agency, Global Network of Isotopes in Precipitation, http://www-naweb.iaea.org/napc/ih/IHS_resources_gnip.html). Stream ^{3}H, used to define C_{out}, was sampled at NB-12 and NB-86 in June 2010 and analyzed at the GNS Science Water Dating Laboratory (Lower Hutt, New Zealand) using electrolytic enrichment and liquid scintillation counting [*Morgenstern and Taylor*, 2009]. The two-parameter exponential-piston flow model was used to approximate $g(\tau)$, such that,

$$\begin{aligned} g(\tau)&=0 && \text{for } \tau<\tau_m(1-f)\\ g(\tau)&=(f\tau_m)^{-1}\exp\left[-\left(\frac{\tau}{f\tau_m}\right)+\left(\frac{1}{f}\right)-1\right] && \text{for } \tau\geq\tau_m(1-f)\end{aligned}. \tag{4}$$

The ratio of exponential volume to the total volume is represented by f and τ_m is the MTT [*Maloszewski and Zuber*, 1982].

3.4. Storage Estimation

We leveraged the Mediterranean-type climate of the Pacific Northwest, USA, with distinct precipitation seasonality, to estimate dynamic storage volumes (mass balance-based storage) for the soil profile (referred to as "dynamic soil storage") and the whole catchment subsurface for both NB-12 and NB-86 (referred to as "dynamic catchment storage"). Assuming a minimum residual soil storage volume at the end of the dry season, dynamic soil storage was calculated as the difference in maximum soil water content and soil water content at the end of the dry season. Similarly, dynamic catchment storage was estimated as the difference between maximum and minimum storage observed over the course of the dry-to-wet transition as calculated using the catchment water balance [e.g., *Sayama et al*., 2011],

$$dV(t)=\sum_{t=1}^{T}P(t)-Q(t)-E(t), \tag{5}$$

where $dV(t)$ is the cumulative change in storage, in mm, from the beginning of the water year (1 October) to time t (h), $P(t)$ is total precipitation (mm), $Q(t)$ is total discharge (mm), and $E(t)$ is evapotranspiration (mm). We computed $E(t)$ using the Penman-Monteith equation [*Monteith*, 1965] and meteorological variables

measured onsite, with the exception of net radiation which was measured at a nearby Ameriflux site (Marys River Fir Site, approximately 28 km northeast of Needle Branch, http://public.ornl.gov/ameriflux/Site_Info/siteInfo.cfm?KEYID=us.oregon_fir.01).

We used stream discharge records and stream water MTTs to approximate total catchment storage, expressed mathematically as,

$$Total\ Catchment\ Storage = MTTi, \tag{6}$$

where i is the mean total annual discharge rate, in mm yr^{-1}, for the period MTT was estimated (years). Deuterium-based MTTs were calculated for NB-12 and NB-86 by convolving the tracer input signal (here the deuterium composition in precipitation, reported as δ^2H), weighted according to the gamma transit time distribution, with the tracer output measured in streamflow [e.g., *Maloszewski and Zuber*, 1982]. Details of field sampling, laboratory analysis, transit time modeling, and uncertainty analysis as well as a discussion of the limitations of this approach are provided in *Hale and McDonnell* [2016]. Tritium-based stream water MTT estimation was described in the previous section (see section 3.3).

3.5. Groundwater Age Estimation

We used tritium/helium-3 ($^3H/^3He$) dating to estimate the apparent age of groundwater sampled at various depths and geomorphic positions within Needle Branch. The dating technique is based on the radioactive decay of ^3H to ^3He, with ^3H having a half-life, $T_{1/2}$, of 12.32 years [*Schlosser et al.*, 1988]. When all other sources of ^3He in groundwater can be accounted for (crustal and mantle sources), a mass balance between the ^3H and the tritiogenic ^3He, $^3He_{trit}$, in a groundwater sample can be used to calculate the time elapsed, $\tau_{^3H/^3He}$, since the sampled parcel of water became isolated from the atmosphere based on the known half-life of ^3H, such that,

$$\tau_{^3H/^3He} = \frac{T_{1/2}}{\ln 2} \times \ln\left(\frac{1 + {}^3He_{trit}}{{}^3H}\right). \tag{7}$$

As a result of the low solubility and high diffusion coefficient of ^3He, exchange of ^3He with soil gas can occur readily within the vadose zone [*Solomon and Cook*, 2000]. Therefore, isolation from the atmosphere is typically not considered complete and, consequently, the $^3H/^3He$ "clock" does not start, until the water has reached the saturated zone.

We collected water and dissolved gas samples from Well-1DP, Well2-DP, Well-8HS, and Well-11FP. In addition, we sampled a well located immediately adjacent to Well-11FP that was not previously described. This well, Well-16SF (SF = surficial), was installed to the soil-bedrock interface at 1 m below the ground surface and the screened interval (0.62–1 m) is located entirely within the soil profile. All wells were purged prior to sampling. The dissolved gas samples were collected with an advanced diffusion sampler [*Gardner and Solomon*, 2009] which was deployed for approximately 72 h following purging. Samples were analyzed for ^3H and dissolved gas concentrations at the University of Utah Noble Gas Laboratory (Salt Lake City, UT).

4. Results

4.1. Hydrodynamic and Deuterium Characterization

Precipitation, specific discharge, precipitation and stream water δ^2H, and groundwater levels for the period of 1 October 2009 to 30 May 2010 are shown in Figure 4. This period covers the duration of the wet season for our Pacific Northwest catchments, including the transition from dry to wet conditions (hereafter referred to as the "wet-up period"). The hydrograph traces in Figure 4a show that the streams responded rapidly to precipitation inputs after the initial wet-up period (a quantitative analysis of the flow regime of these catchments is provided in *Hale and McDonnell* [2016]). Specific discharge was higher at the smaller NB-12 catchment during most runoff events, however, the mean difference in specific discharge between the catchments during the period shown was only 0.04 mm h^{-1}.

Despite the highly responsive rainfall-runoff dynamics of these catchments, the δ^2H signal in stream water was substantially damped relative to the variability of δ^2H measured in precipitation (Figure 4b). The standard deviation of stream water δ^2H was 1.8‰ for NB-12 and 2.2‰ for NB-86 over the entire period of record while the standard deviation of precipitation δ^2H was 15.1‰ (Table 1).

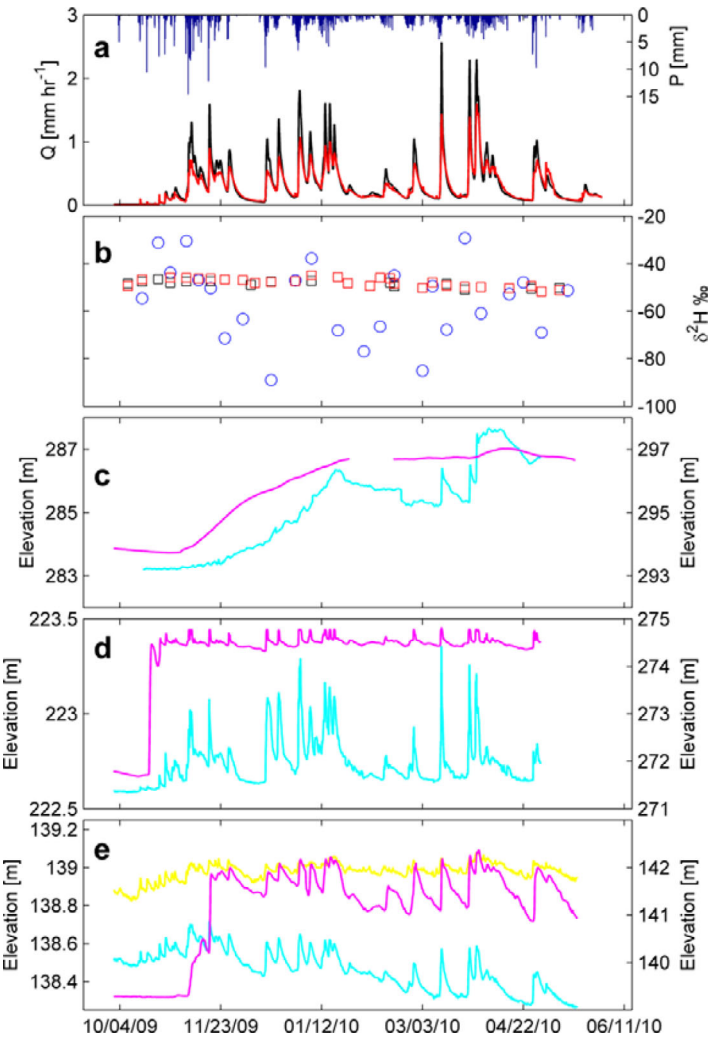

Figure 4. Hydrometrics and tracer dynamics measured from 1 October 2009 to 30 May 2010. Precipitation (blue) and specific discharge for NB-12 (black) and NB-86 (red) is shown in Figure 4a. Deuterium composition of precipitation (blue circles), NB-12 stream water (black squares), and NB-86 stream water (red squares) is shown in Figure 4b. Water level elevations Well-1DP (cyan, left axis) and Well-2DP (magenta, right axis) are shown in Figure 4c. Water level elevations for Well-3HS (magenta, right axis) and Well-8HS (cyan, left axis) are shown in Figure 4d. Water level elevations for Well-9HS (magenta, right axis), Well-10FP (cyan, left axis), and Well-11FP (yellow, left axis) are shown in Figure 4e.

Each of our two deep wells displayed unique water level dynamics during the 2010 wet season (Figure 4c). Although water levels in both wells increased in elevation by approximately the same absolute value (roughly 4 m), Well-1DP was distinctly more sensitive to precipitation events than Well-2DP. At Well-2DP, the water table increased gradually over the course of the wet season whereas, at Well-1DP, many short-term fluctuations occurred as the water level increased. Hillslope wells, Well-3HS (Figure 4d) and Well-9HS (Figure 4e), were both nonresponsive during the early wet-up period but began to rapidly rise to a new base level after 59 and 222 mm of accumulated precipitation, respectively. Once activated, these wells responded rapidly to precipitation throughout the remainder of the wet season. The other hillslope well, Well-8HS, did not display a threshold-type behavior prior to responding to precipitation. Instead, its water level closely mimicked the dynamics of the stream for the entire wet season, including the wet-up period (Figure 4d). Both floodplain wells, Well-10FP and Well-11FP (sealed into the bedrock below the alluvial sediments), were responsive to precipitation

Table 1. Mean Deuterium Composition and Standard Deviation (or Range, Indicated by Asterisk, for Small Sample Sizes) of Precipitation, Stream Water, and Groundwater (Parentheses Represent the Values for Only the Time Period Shown in Figure 4b)

Location	Mean δ^2H (‰)	δ^2H Standard Deviation or Range	n
Amount-weighted precipitation	−50.6 (−57.3)	15.1 (16.4)	170 (24)
NB-12	−49.6 (−48.4)	1.8 (1.3)	108 (15)
NB-86	−50.1 (−48.0)	2.2 (1.9)	179 (27)
Well-1DP	−51.2	1.4*	8
Well-2DP	−52.0	1.9*	2
Well-3HS	−49.7		1
Well-8HS	−50.6	2.2*	2
Well-9HS	−48.3	1.2*	2
Well-10FP	−50.5	2.3*	3
Well-11FP	−50.8	0.9*	4
Well-16SF	−48.4	6.3*	12

Table 2. Soil Water Mean Transit Time Modeling Results[a]

Site	$D_{p\text{-mle}}$	$D_{p\text{-}10/90\%}$	$\tau_{m\text{-mle}}$ (days)	$\tau_{m\text{-}10/90\%}$ (days)	NSE_{mle}
Midslope	0.06	(0.05/0.48)	132	(96/134)	0.57
Toeslope	0.59	(0.54/0.66)	63	(59/69)	0.79

[a]Maximum likelihood estimates (mle) for the dispersion parameter (D_p) and mean transit time (τ_m) parameter of the dispersion flow model, parameter uncertainties, and Nash-Sutcliffe efficiencies (NSE) are presented. Both locations represent 0.5 m soil depths.

during the wet-up period and throughout the wet season, but the range of fluctuations were less than 0.5 and 0.2 m, respectively, over the entire period.

We did not sample the wells during the 2010 wet season since the act of taking a sample would disrupt the water level record and obscure interpretation. We did, however, collect samples for isotopic analysis prior to this period. Table 1 provides the mean δ^2H values and standard deviations (or ranges, where sample size is small) for the sampled groundwater. The mean values for all groundwaters were within 2‰ of the mean precipitation and stream water values (analytical error = 1‰). Similar to stream water, the groundwater δ^2H values at all locations except Well-16SF did not vary significantly (a range of 6.2‰ was measured at Well-16F whereas the range for all other locations was less than 2.5‰).

4.2. Soil Water MTT

The maximum likelihood MTT estimate for soil water collected at the midslope lysimeter was 132 days (Table 2). The toeslope MTT was approximately half of the midslope value (63 days). At both locations, the model performed reasonably well (Nash-Sutcliffe efficiencies of 0.57 and 0.79, respectively). The tenth and ninetieth percentile MTT estimate from the log likelihood uncertainty estimation procedure (see *Hale and McDonnell* [2015] for a detailed description of the method, its assumptions, and limitation) produced an uncertainty range of 38 days for the midslope lysimeter (96–134 days) and 10 days for the toeslope lysimeters (59–69 days).

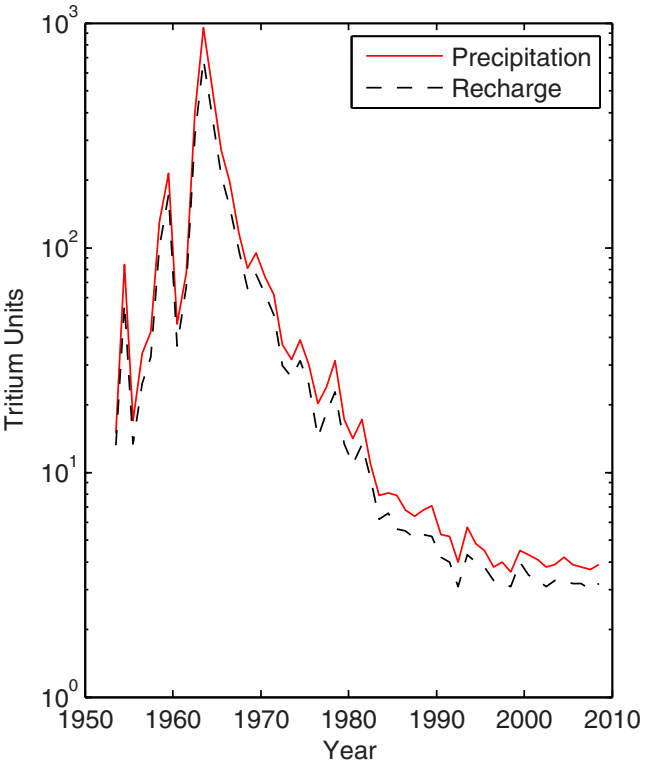

Figure 5. Estimated annual mean tritium concentrations in precipitation based on Portland, Oregon measurements, and the associated tritium input function (recharge) used in ^{3}H-based MTT calculations.

4.3. ^{3}H-Based Stream Water MTT

Mean transit times were estimated from single stream water ^{3}H values at NB-12 and NB-86 and the estimated tritium input function (Figure 5) by iteratively adjusting the two parameters of exponential-piston flow model, f and τ_m (where τ_m =MTT), until the parameter set that best matched the measured ^{3}H concentration of the sample to the model output, C_{out}, was identified. The a priori parameter distributions were $0 \leq f \leq 1$ and $0 < \tau_m \leq 100$ years. For both NB-12 and NB-86, the best fit was found for $f = 0.7$ (Table 3) although f values from 0.4 to 0.8 all provided similar MTT estimates. The best fit ^{3}H-based MTTs were 6.8 and 7.7 years for NB-12 and NB-86, respectively; but because of the uncertainty associated with this approach, we used the lower and upper bounds of the MTT estimates (reported in Table 3) in our storage analysis.

Potential uncertainty sources in our MTT estimates are sample

Table 3. Tritium-Based Mean Transit Time Results With Deuterium-Based Transit Times Provided for Comparison (Samples Collected on 10 June 2011)

Location	Model	Exponential Fraction, f	^{3}H-Based MTT (years)	δ^2H-Based MTT (years)
NB-12	EPM	0.7	6.8 (5.1/8.5)	5.0 (4.0/8.7)
NB-86	EPM	0.7	7.7 (6.0/9.4)	4.0 (3.5/4.9)

measurement error, error in our flow model, and/or error in the input function. The sample measurement error was ±0.04 TU, which is associated with an MTT error of ±0.4 year. If we assume the error in the flow model estimation was ±10% (i.e., $f = 0.7 \pm 0.10$), the associated MTT error is ±0.5 year. Errors in the input function result from sample measurement error for precipitation, correlation errors with the Vienna precipitation record used to fill data gaps in the Portland, Oregon precipitation time series, and errors estimating the recharge weighting function, together estimated to total ±0.2 TU which corresponds to a MTT error of ±1.6 years. Assuming these three error sources are independent, the overall MTT error was ±1.7 years. This value was applicable to both NB-12 and NB-86 since both samples were subject to the same error sources. General assumptions and limitations of the lumped-parameter approach for MTT estimation are discussed in *Hale and McDonnell* [2016].

4.4. Soil and Catchment Storage Estimates

Soil water content from a representative soil profile was used to estimate the dynamic soil storage available across the catchments. Figure 6 shows stream discharge as a function of soil water content during the course of the wet season, including the wet-up period (see inset for the source data time series). The instantaneous maximum value of stored soil water was 235 mm during this measurement period, while the dynamic soil storage was 120 mm (maximum storage minus baseline storage at beginning of measurement period). A threshold behavior was evident in the stream discharge versus soil water relationship, whereby stream discharge did not commence until soil moisture storage reached 180–200 mm. This threshold value represents 77–85% of the maximum soil storage (235 mm) for our measurement period.

Cumulative change in storage volume, dV, since the beginning of each water year of record was estimated for NB-12 and NB-86. Figure 7 shows stream discharge as a function of dV for NB-12 (a) and NB-86 (b). Runoff generation occurred across a range of dV values at both catchments, except approximately the lowest

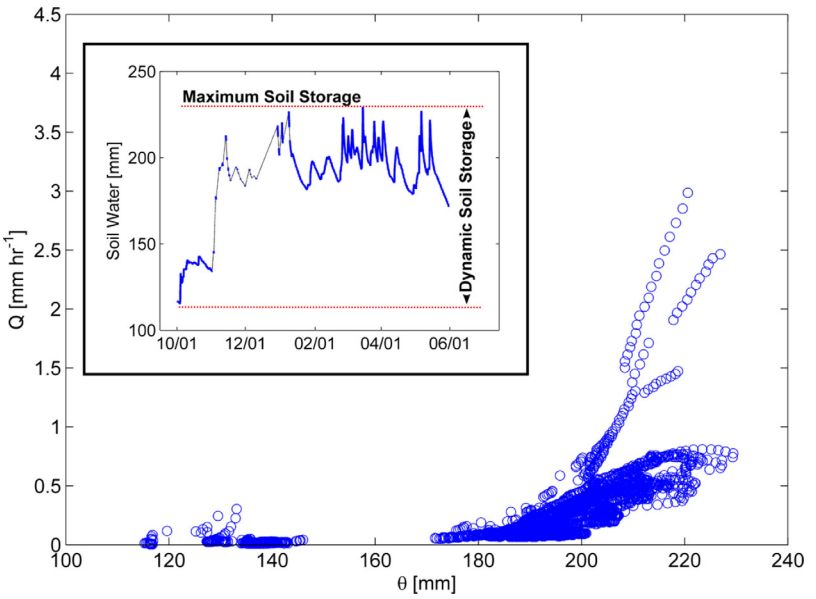

Figure 6. Stream discharge at NB-86 as a function of soil water content. Water depth is estimated using the integration of measurements obtained from four soil moisture sensors distributed within a 1 m deep soil profile (0.15, 0.35, 0.65, and 0.85 m depths). The inset shows the times series of soil water depth calculated during the course of the wet-up and wet periods at a representative hillslope profile that was used to construct the main figure. The dashed black line in the inset represents values interpolated to fill data gaps (not used in the analysis shown in the main figure).

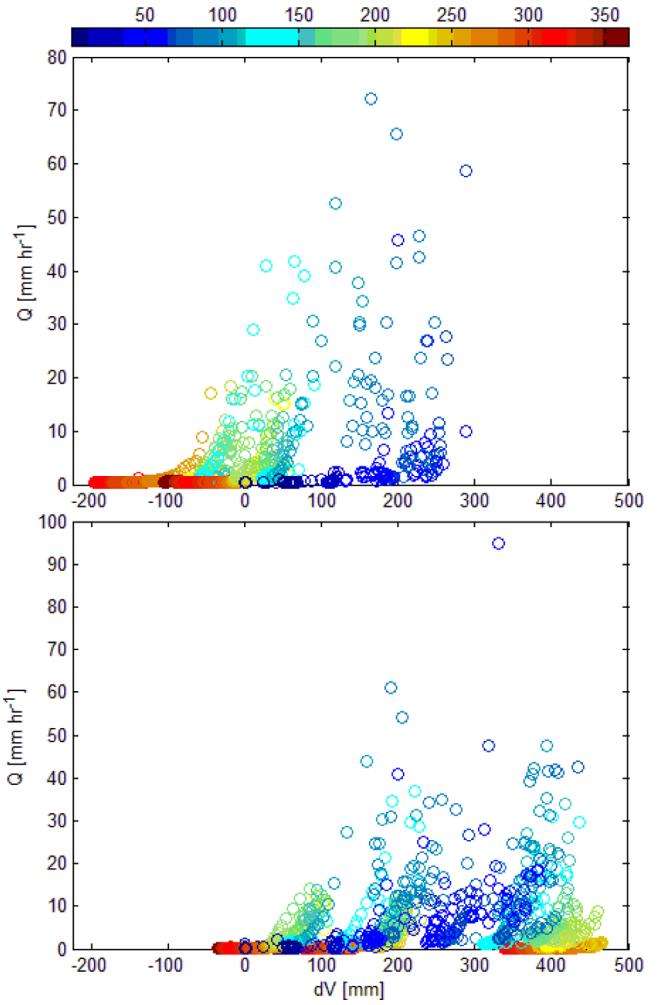

Figure 7. Discharge as a function of change in storage (dV) since the beginning of the water year for (a) NB-12 and (b) NB-86. Marker color represents the day of the water year.

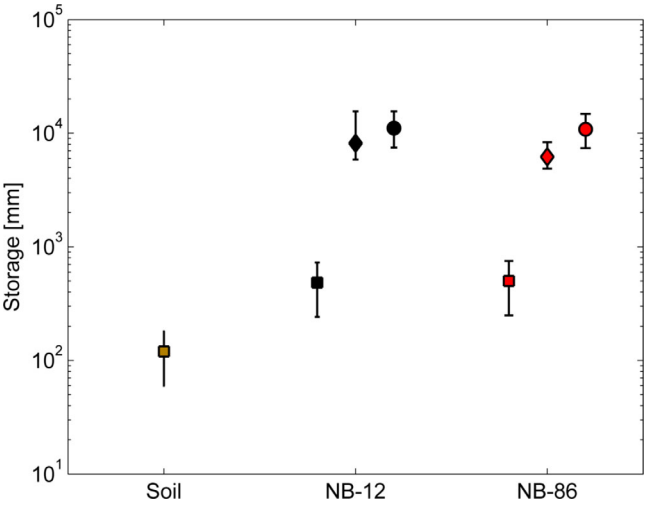

Figure 8. Comparison of dynamic (squares) and total storage (deuterium-based estimates are represented with diamonds and tritium-based estimates are represented with circles) for the soil profile (brown), NB-12 (black), and NB-86 (red).

100 mm interval. This "threshold" value aligns well with our estimate of 120 mm of soil profile dynamic storage. Catchment dynamic storage, taken as the absolute difference between the maximum *dV* and minimum *dV* measured during the period of record, was 485 mm for NB-12 and 501 mm for NB-86.

We used MTT estimations derived from both stable isotope (δ^2H) and ^{3}H values of NB-12 and NB-86 stream water to estimate total catchment storage (Figure 8; dynamic catchment storage estimates are also plotted for comparison). As a result of the uncertainty associated with the MTT estimations, we used a conservative approach to calculate the potential range of total catchment storage. The lower bound of the MTT estimate was multiplied by the lower bound of the mean of the total annual discharge values (taken as mean total annual discharge minus 10%) for the period of record used in the MTT estimation to estimate the lower limit of total catchment storage. Likewise, the upper bounds of the MTT estimate and mean of the total annual discharge (mean plus 10%) were used to define the upper limit of total catchment storage. The resulting ranges of total catchment storage for NB-12 were 5900–15,600 mm based on the δ^2H MTT estimate and 8500–13,300 mm based on ^{3}H. At NB-86, total catchment storage is estimated to range from 4900 to 8400 mm (δ^2H) and 8400 to 13,100 mm (^{3}H). The close agreement of both MTT-based catchment storage estimates (δ^2H and ^{3}H based) is evident in Figure 8. Total catchment storage for both NB-12 and NB-86 is more than an order of magnitude larger than dynamic catchment storage.

4.5. Groundwater Ages

We used ^{3}H/^{3}He dating to estimate groundwater ages at five wells within the NB catchment (locations shown in Figure 9). Tritiogenic ^{3}He used in equation (7) was computed by subtracting the ^{3}He due to equilibrium solubility,

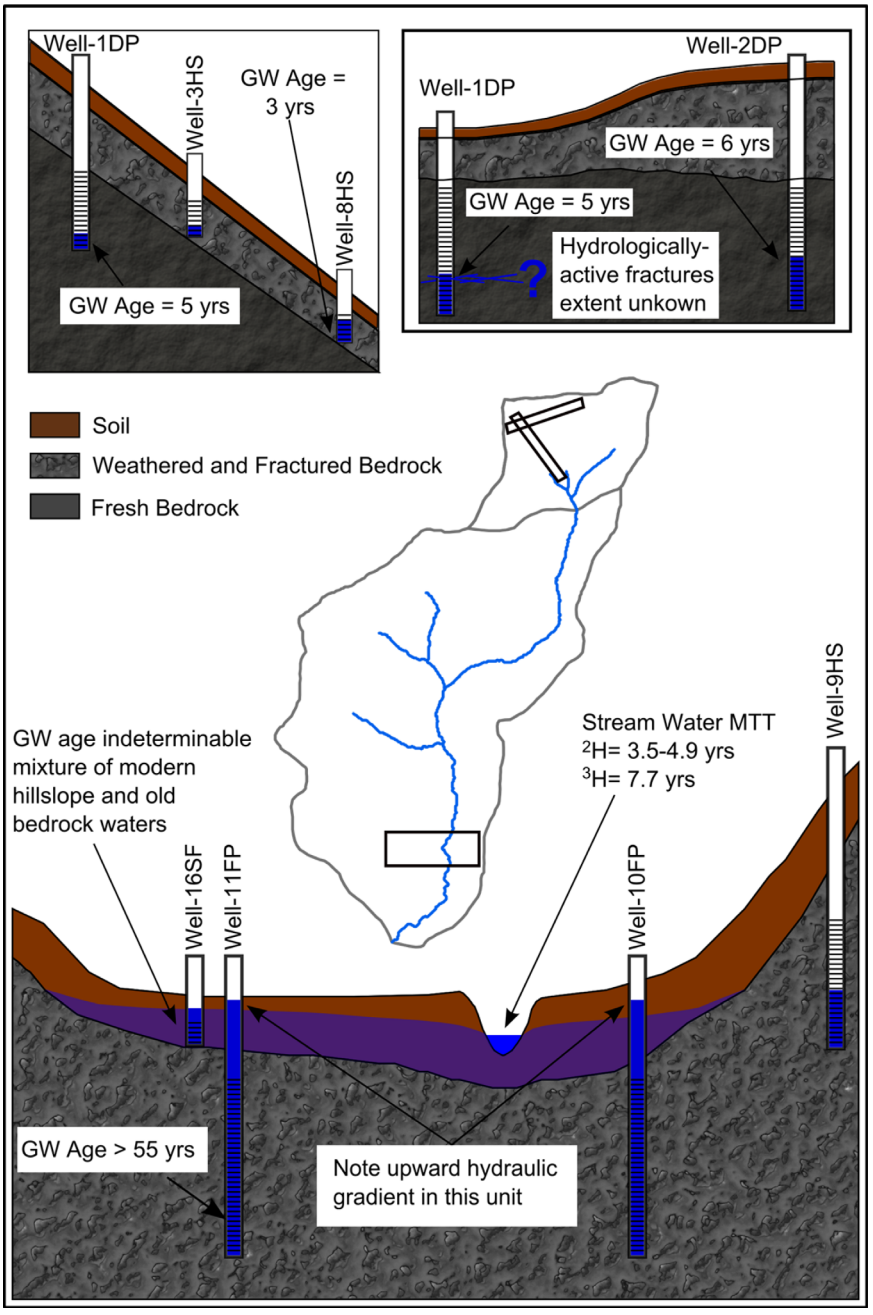

Figure 9. Diagram showing groundwater ages.

excess air, and from terrigenic sources. The amount of excess air was estimated using the closed equilibrium model (CE) [*Aeschbach-Hertig et al.*, 1999]. Terrigenic ^{3}He was computed using ^{4}He in excess of solubility and an assumed ^{3}He/^{4}He ratio of 2×10^{-8} for the terrigenic helium (Rterrigenic). Noble gas and tritium data are shown in Table 4.

Most of the samples have noble gas concentrations that are near atmospheric solubility at a temperature of about 9°C. As a result, the amount of excess air is relatively small. The sample from Well-2DP has noble gas concentrations below atmospheric solubility apparently as a result of a minor amount of gas stripping in the subsurface. Only the sample from Well-1FP has significant amounts of terrigenic He. The uncertainty in the apparent ^{3}H/^{3}He age was computed using a Monte Carlo approach that randomly varied the amounts of Ne, ^{4}He, R/Ra, Rterrigenic, and the atmospheric pressure within 1 standard deviation of the uncertainty of

Table 4. Noble Gas Tritium and Apparent Age for Well Samples

Sample	^{4}He (ccSTP/g)× 10^{-8}	Ne (ccSTP/g) × 10^{-7}	Ar (ccSTP/g) × 10^{-4}	Kr (ccSTP/g) × 10^{-8}	Xe (ccSTP/g) × 10^{-8}	R/Ra[a]	^{3}H (TU)	App. Age (year)	Age Uncert. (year)
Well-1DP[b]	4.57	1.97	3.79	9.11	1.32	1.009	1.70	4.3	3
Well-8HS[b]	4.5	1.95	3.80	9.27	1.36	1.002	1.25	0	2
Well-2DP[b]	3.67	1.57	3.07	7.72	1.11	1.009	2.24	NA[c]	NA[c]
Well-11FP[d]	14.0	2.47	4.51	1.04	1.53	2.236	0.45	>55	
Well-16SF[e]	4.79	2.21	4.21	9.13	1.37	0.986	1.44	0	3

[a]R is the ^{3}He/^{4}He ratio of the sample while Ra is the ^{3}He/^{4}He ratio of the air standard (1.384×10^{-6}).
[b]Sampled on 20 August 2010.
[c]An apparent age was not computed because gas stripping has removed gas.
[d]Originally sampled on 20 August 2010, but gas sample was compromised and resampling was required (collected on 19 April 2011). The ^{3}H value measured on 20 August 2010 was 0.29 TU.
[e]Sampled on 19 April 2011.

each of these parameters. The uncertainty in apparent age is large for most of the samples because the small amount of tritium in precipitation gives rise to only small amounts of tritiogenic ^{3}He, especially when the waters are first isolated from the atmosphere (i.e., when the waters are young, the fraction of the total ^{3}He that is from tritium decay is small). Furthermore, the ^{3}H/^{3}He "clock" does not record the transit time in the unsaturated zone and this is likely to include the region above the seasonal low water table that is saturated after wet periods.

Groundwater was youngest (2.8 ± 2.3 years) in Well-8HS, which is located approximately 10 m (horizontal distance) from the stream and integrates fractures occurring in the bedrock between 2.5 and 5.7 m below the ground surface. The groundwaters in Well-1DP and Well-2DP were approximately 2 years older than the shallow bedrock water in Well-8HS (5.0 ± 1.8 and 5.8 years, respectively; the uncertainty calculation was not possible for Well-2DP). Lower in the catchment, the bedrock groundwater below the alluvial floodplain was greater than 55 years old (Well-11FP; an exact age was not possible given its extremely low, prebomb era ^{3}H concentration). Age determination for Well-16SF, the surficial aquifer immediately overlying the Well-11FP unit, was not possible but the sample appeared to be a mixture of modern and old water based on the ^{3}H concentration (intermediate to the old groundwater below it and the younger, shallow bedrock groundwater in Well-8HS) and because the ratio of ^{3}H/^{3}He in the sample was the same as the ^{3}H/^{3}He ratio of the atmosphere. The interpretation of mixed water in the surficial aquifer is supported by hydrometric measurements that showed an upward, vertical hydraulic gradient for the underlying bedrock groundwater (see depiction in Figure 9).

5. Discussion

5.1. Subsurface Storage Characterization: The Bottom-Up Approach

We used a multipronged approach to investigate the subsurface storage controls on stream water MTT and MTT scaling in the permeable sandstone catchments studied by *Hale and McDonnell* [2016]. By combining direct interrogation of the subsurface through borehole characterization and groundwater monitoring with tracer-based dating techniques, we identified discrete storage zones that influence stream water MTT. Although a continuous system, our bottom-up approach noted five zones with distinct storage controls:

1. **Soil Zone.** Defined as the pore space in the soil and subsoil available to hold water. This soil water retention can be short as evidenced by our lysimeter-based MTT estimates for soil water on the order of 60–130 days.
2. **Shallow Bedrock Zone.** Includes the saprolite and highly, fractured upper layer bedrock. Based on our borehole data, the thickness of this storage zone likely ranges from a couple of meters to over 10 m.
3. **Deep Bedrock Zone.** Consists of storage available in rock matrix and fractures in bedrock below the shallow bedrock zone. The lower boundary of this storage zone is unknown.
4. **Surficial Alluvial Zone.** Comprised of the soil and alluvial and colluvial sediments lying above the bedrock in the alluvial plain. The soil texture in the alluvial plain grades from a loam at the surface to a silty

clay at depth, inducing at least partial saturation of the profile for most of the year and creating an aquitard between the surficial alluvial zone and the last identifiable storage zone.

5. **Suballuvial Zone.** Storage held in the weathered and fractured bedrock lying immediately below the surficial alluvial zone; the depth of this zone is unknown, but it is at least 5 m thick based on our borehole data.

Storage volume in the soil zone is small relative to estimates of total catchment storage. Maximum soil storage during our measurement period was 235 mm, compared to total catchment storage estimates on the order of 10,000 mm. This ratio of soil water storage to total catchment storage is very different to the more traditional poorly permeable headwater research catchment, where soil water storage is the largest of all the storages in the system (see *Sayama and McDonnell* [2009] for review). Our maximum soil storage estimate is based on a single wet-season and is therefore best taken as an approximate maximum storage. Notwithstanding the implicit uncertainty in these soil storage calculations, both are extremely small relative to total catchment storage. The threshold behavior between soil storage and stream discharge indicates that, in most cases, storage deficits in the soil profile must be satisfied before runoff is generated (a common finding in headwater systems [*Western et al*., 2002]). Water storage within the soil is highly transient relative to the groundwater storage zones, with MTTs estimated between 60 and 130 days. Water flow direction in the same soil type at the nearby Mettman Ridge site was exclusively vertical under all wetness conditions [*Torres et al*., 1998]. We therefore view the soil profile as a temporary storage zone that regulates vertical recharge to the shallow bedrock zone immediately below.

Groundwater dynamics in the shallow bedrock zone varied among our three wells, indicating heterogeneity in the storage properties of this zone. Such heterogeneity is expected in highly fractured rock aquifers [*Freeze and Cherry*, 1979]. Two of the hillslope wells (HS series) did not respond immediately to precipitation during the wetting-up period, but after a presumable storage deficit was replenished, the groundwater increased rapidly to a new base water level and became responsive to further precipitation inputs (Figure 4). This delayed, threshold-like response was also observed in shallow bedrock groundwater at the Mettman Ridge hillslope [*Anderson et al*., 1997b; *Montgomery et al*., 2002] and fits the *Sidle et al*. [2001] hydrogeomorphic conceptual model whereby different geomorphic units become hydrologically active with increasing antecedent wetness. Well-8HS behaved differently than the other two hillslope wells, closely matching the dynamics of streamflow independent of antecedent conditions. In combination with the observed groundwater dynamics, extended pumping of Well-8HS, at rates of up to 2 L min^{-1} during the late-summer (i.e., driest antecedent conditions), provided convincing evidence that this borehole intersects perennially water-bearing fractures that are tightly connected to the stream. The groundwater in this well was younger than the MTT of the stream water approximately 100 m downstream at NB-12 (3 years versus 5 years), indicating that other (and older) storage components contribute to streamflow at the small, 12 ha catchment scale.

Groundwater dynamics in our two deep bedrock wells displayed different characteristic behavior, similar to the heterogeneity observed in the shallow bedrock wells. Water levels in both deep wells increased over the course of the wet-season (Figure 4). However, the responsive nature of Well-1DP suggests that the water-bearing fractures mapped at 30–35 m depth in this borehole are indeed hydrologically relevant on the time scale of individual storm events. While the responses are likely expressions of pressure wave propagation through a hydraulically primed fracture network [*Rasmussen*, 2001], the time scale of the response indicates an intimate connection between the surface and deeper storage zones under wet antecedent conditions. The groundwater dynamics in Well-2DP are much more subdued, following a gradual increase over the course of the wet season with no response to individual precipitation events (indicating the behavior of bedrock groundwater in the absence of hydrologically active fractures). Despite the dissimilarities in water level dynamics on short time scales, the age of the groundwater in these two wells is similar; 5 and 6 years for Well-1DP and Well-2DP, respectively. The groundwater elevation in Well-2DP is, on average, 10 m higher than the water surface elevation in Well-1DP 150 m away. With a depth differential of only 10 m at 150 m distance and similar ages, we expect that we are measuring the same groundwater storage component. It is also likely that stored water in the deep bedrock zone contributes to streamflow, as inferred from the mixing with the younger, shallow bedrock water necessary to achieve the stream water MTT measured at NB-12.

Groundwater in the suballuvial zone is the first to exhibit a response to precipitation inputs early in the wetting-up phase, reacting even before the stream begins to respond to precipitation. We believe this

storage zone is semiconfined as a result of the silty clay aquitard located at the base of the soil profile in the alluvial plain. The piezometric surface confirms some level of confinement in this unit as it is always above the elevation of the free water surface in the surficial alluvial zone (not shown), and becomes artesian during larger storm events. The ^{3}H concentration, as well as evidence from dissolved silica analysis and specific conductivity measurements made at the time of ^{3}H sampling, confirm that this is a distinctly different pool of water than that present in the surficial alluvial zone above it. The ^{3}H concentration was 0.45 tritium units (TU) in the suballuvial zone compared to 1.46 TU in the surficial zone; the silica concentration was 10.2 mg L^{-1} and specific conductivity was 264 μS cm^{-1} in the suballuvial groundwater (Well-11FP) compared to 4.46 mg L^{-1} and 34 μS cm^{-1} in the surficial alluvial groundwater (Well-16SF). This distinction was not evident based on the δ^2H and δ^{18}O values of the two water pools (see similar values in Table 1). At greater than 55 year old, the water in the suballuvial zone is considerably older than any of the other storage zones we identified. This finding links directly to the issue of truncation of stable isotope-based MTT reported by *Stewart et al*. [2010] and *Frisbee et al*. [2013]. If multiple tracers were not employed, we would not have been able to discriminate this zone from the surficial alluvial zone above. Of course, we acknowledge that it is possible that we are missing water yet another order of magnitude older as observed by *Frisbee et al*. [2013] in spring water of the San Juan Mountains of southern Colorado, USA (funding for radiocarbon dating was outside of the budget of our project). The use of additional tracers capable of interrogating old (hundreds to thousands of years) groundwater, such as those described in *IAEA* [2013], may have further improved our ability to discretize and characterize the age distributions of these waters.

Groundwater dynamics for the surficial alluvial zone are not available for the measurement period shown in Figure 4 as a result of instrument failures. However, monitoring from previous years shows that the water table dynamics closely follow the stream (not shown). Groundwater age dating was inconclusive but the ratio of the sample ^{3}H concentration to the ^{3}H concentration of the atmosphere showed strong evidence of mixing of old suballuvial and more modern hillslope water. The surficial alluvial zone therefore acts as a mixing tank, combining water from two distinctly different storage reservoirs prior to discharging it to the stream. Similar mixing of old and young water has been reported in forested lowland catchments in Costa Rica [*Solomon et al*., 2010], glacially formed catchments in the Scottish Highlands [*Birkel et al*., 2014; *Soulsby et al*., 2015; *Tetzlaff et al*., 2014] and in a montane, subtropical catchment in Australia [*Duvert et al*., 2016].

5.2. Subsurface Storage Ages and MTT Scaling

Our results suggest that the bedrock permeability (and more specifically, the permeability structure with depth) in the sedimentary catchments of the Oregon Coast Range creates a groundwater flow system where streamflow in the smaller catchments is fed primarily by local groundwater flow from the shallow and deep bedrock zones (Figure 10a). As catchment scale increases, contributions from the surficial alluvial and suballuvial zones become important. The suballuvial zone is conceptualized as a landscape-scale storage reservoir that is recharged through the deep fracture network (Figure 10b). The surficial alluvial zone integrates young and local shallow bedrock groundwater moving laterally through the adjacent hillslopes with the older, deep, local-scale groundwater upwelling from below the valley-bottom. The proportions of young hillslope groundwater and old valley-bottom groundwater combining in this critical mixing zone set the MTT of the groundwater discharging to the stream (Figure 10c). Base flow MTT is then set by the mixing of stream water already in the channel with local groundwater inflow.

The MTT scaling observed in our permeable bedrock catchments, whereby stream water MTT increases with catchment area, appears largely controlled by increased contributions of long flow path, suballuvial groundwater to the surficial alluvial mixing zone in the downstream direction. This general conceptualization of deeper and older water sources increasing in a downstream direction is consistent with the findings of *Frisbee et al*. [2011] in a 1600 km^2 alpine catchment in southern Colorado. Additionally, *Personious* [1995] showed that stream channel incision into the bedrock proceeds in a downstream direction in Oregon Coast Range streams (Drift Creek was included in his study). As the channel cuts closer and/or into the underlying suballuvial zone, contributions from this zone would be expected to increase based on such a geomorphological rationale; leading to concomitant increases in stream water MTTs with increasing catchment area.

The multicomponent storage system we find in the permeable sedimentary bedrock at our Oregon Coast Range catchments contrasts with the much simpler storage system in the volcanic HJA catchments as described in *Hale and McDonnell* [2016]. The low-permeability volcanic bedrock restricts storage to the soil

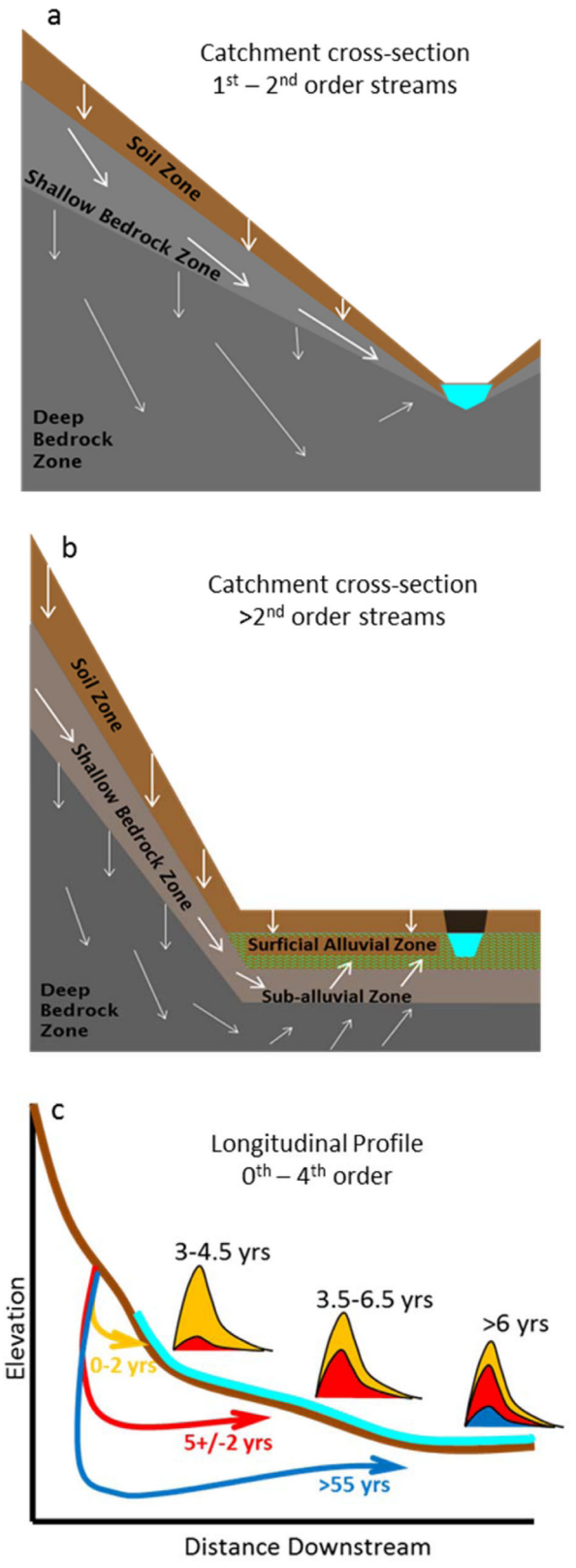

Figure 10. Conceptual diagrams of subsurface flow paths (a) in zero-order to first-order catchments without alluvial plain morphology, (b) in second-order and greater catchments, and (c) as viewed longitudinally with approximation of subsurface transit time ranges and consequential stream base flow mean transit times.

profile on the HJA hillslopes. Recent borehole investigations by *Gabrielli and McDonnell* [2011] indicate some potential for storage in shallow fractures in the volcanic bedrock of the HJA. However, there is little vertical connectivity below this thin, fractured zone and effectively impermeable rock below, so this storage zone likely has less of an effect on setting stream water transit times and more influence on controlling the precipitation threshold for stream response as observed by *Graham and McDonnell* [2010]. Indeed, detailed, bottom-up investigations at the HJA [*Harr*, 1977; *McGuire and McDonnell*, 2010] show the strong permeability contrast between the soil and bedrock results in precipitation-induced development of a thin, transient zone of saturation at the soil-bedrock interface which moves laterally downslope as gravity-driven flow. These gravity-driven and topographic-driven runoff processes relate directly to the relatively short MTTs and MTT relationships with flow path length and gradient observed at the HJA catchments [*McGuire et al*., 2005]. Although surficial alluvial zones exist in catchments at the HJA that have valley-bottom morphology [*Swanson and James*, 1975], the MTTs presented in *McGuire et al*. [2005] suggest that storage within the surficial alluvial zone does not significantly affect catchment transit time distributions. This is shown clearly by the similarity in stream water MTTs at WS10 (1.2 years), which has no riparian storage, and WS03 (1.3 years), where *Wondzell* [2006] documented storage within the alluvial and colluvial sediments that fill the valley bottom. The sharp permeability contrast at the soil-bedrock interface created by the high-conductivity soil overlying low-conductivity hydrothermally altered volcanic rock at the HJA results in a system where storage is relegated to the soil profile and runoff processes and stream water MTTs are driven by topography.

The contrasts in landscape-scale anisotropy may in fact be the simplest way to differentiate our findings in these two broad classes of catchments: low landscape anisotropy in the permeable Oregon Coast range, where no mechanism exists, such as the sharp permeability contrast at the soil-bedrock interface at HJA, to induce lateral subsurface

flow [*Bonell and Bruijnzeel*, 2004], to high landscape-scale anisotropy at HJA whereby such a mechanism is present and controls runoff generation throughout the wet season. This finding is directly linked to *Asano and Uchida*'s [2012] finding that MTT magnitude was related to the depth of the hydrologically active zone for a smaller range of catchment scales and in a different rock type (granite). Further, we show the consequences of the process dynamics developed at hillslopes scales at the nearby Mettman Ridge sites (including *Montgomery et al*. [1997], A*nderson et al*. [1997b], *Torres et al*. [1998], *Montgomery et al*. [2002], and *Montgomery and Dietrich* [2002]) across catchment scales extending to 100 km^2.

While time-invariant MTT estimates were used here to discern multiple catchment storage components, the resulting conceptualization paired with observed nonlinear hillslope, groundwater response (Well-9HS), and soil moisture-stream discharge relationships suggests that the true MTT is likely highly dynamic (i.e., time variable). This hypothesis is supported by the findings of both *Heidbüchel et al*. [2013] and *Soulsby et al*. [2015] whereby catchment wetness controlled the number and magnitude of active storage components with commensurate implications for stream MTT. Modeling by *Birkel et al*. [2014] indicated that MTTs in a Scottish Highland catchment displayed the greatest degree of time-dependent variation during extreme wet and dry conditions as a result of a large riparian storage reservoir acting to filter variability under average conditions. Given the number of storage components identified at our sites and that the surficial alluvial zone that mediates mixing is not disproportionally large relative to the other storage components, we hypothesize that MTT likely varies more continuously throughout the course of the annual wetting and drying cycles as the various stores fill and release. As MTTs are known to be sensitive to mixing processes [*Fenicia et al*., 2010; *Botter*, 2012; *van der Velde et al*., 2014], the ability to infer the primary mixing zone and contributing stores through our combined hydrometric-tracer approach is particularly important to developing the process-based link between catchment storage and MTT scaling relationships for our catchments.

5.3. Dynamic Versus Total Storage Volumes

Total storage at NB-12 and NB-86 was an order of magnitude larger than the water balance-derived dynamic storage estimations (soil and catchments). Neither total nor dynamic storage showed a dependence on catchment scale. Many factors contribute to uncertainty in our storage estimates, such as hydrometric measurement errors, soil depth and porosity heterogeneity, and MTT uncertainty. Even accounting for considerable uncertainty in our estimations (we conservatively estimated uncertainty as $\pm$50% of the calculated dynamic catchment storage estimate), total catchment storage is still significantly larger than dynamic catchment storage (10^3-10^4 versus 10^2, respectively) at both NB-12 and NB-86 (Figure 8). While this difference seems extreme, *Birkel et al*. [2011a] also observed order of magnitude differences in dynamic and total storage at two catchments in the Scottish Highlands. They attributed the relatively small dynamic storage to a combination of thin hillslope soils overlying impermeable bedrock and highly responsive valley-bottom soils that overlie poorly permeable glacial till. The relatively larger total storage is a result of the overall volume of saturated soil present in the wide, glacially carved valley. At our Oregon Coast Range catchments, the dynamic soil storage (approximately 120 mm) in combination with the amount of precipitation necessary to activate shallow bedrock groundwater in two of our shallow bedrock wells (60 and 220 mm) is in close agreement with the catchment-scale dynamic storage estimates (485 and 500 mm for NB-12 and NB-86). Since dynamic storage is relatively small and can essentially be accounted for by storage in the shallow subsurface, the considerable total storage volume is likely achieved by a continually full deeper fracture system.

Sayama et al. [2011] linked the dynamic storage volume of various-sized catchments in coastal northern California to the mean catchment slope angle, suggesting that steeper catchments were capable of storing greater volumes of water in the hydrologically active bedrock. At our site, NB-12 is significantly steeper than NB-86 (median slope of 51 versus 34%, respectively); however, the dynamic storage estimates are relatively similar (within 15 mm). Although our sample size is small, our results do not support the *Sayama et al*. [2011] hypothesis. The lower slope angles in NB-86 are linked to a past history of large deep-seated landslides that have not occurred in NB-12. It is possible that, during the course of the landslide, any loss of storage associated with the size of the overall control volume (based on high slope angles) was offset by an increase in the volume of void space created during fracturing and crumbling of bedrock during the slide. Given the importance of subsurface storage outlined in this study, the role of deep-seated landslides in controlling catchment storage is an interesting, and open question in the hydrology of our system.

6. Conclusions

In this paper, we showed the importance of bedrock permeability in controlling stream water MTTs and MTT scaling relationships. We found that the permeable sedimentary bedrock in our Oregon Coast Range catchments led to the development of distinct zones of storage. Our hydrometric, MTT, and groundwater dating analyses showed that stream water MTTs were controlled by a mixture of water contributions from the individual zones within the permeable bedrock. We provide strong evidence that the relative contributions from each storage component change with catchment area and lead to the observed MTT scaling behavior. Without our bottom-up, process-based approach—employing multiple tracers and dating methods—this mechanistic understanding of how MTTs are controlled and scaled based on catchment storage characteristics would not have been possible. Our work suggests that the permeability distribution in the subsurface represent perhaps the most basic control on how water is stored within the subsurface and therefore is perhaps one of the best direct predictors of stream water MTT (i.e., more than previously derived morphometric-based predictors).

Efforts are underway within the hydrological research community to derive a catchment classification system [*McDonnell and Woods*, 2004; *Wagener et al*., 2007; *McDonnell*, 2013]. As inclusion of catchment function (collection, storage and discharge) into any classification scheme is important, our work is relevant to these efforts in several ways. First and foremost, functional representation requires thorough understanding of the underlying geology and, more specifically, how the bedrock lithology and structure create widely varying flow paths and storage zones within the subsurface. Furthermore, our work suggests that indices of catchment form and rainfall-runoff response are incomplete descriptors of catchment function as they do not fully account for catchment storage. Our overarching message is that catchment function is more than skin-deep and efforts to classify or group catchments should begin to include such metrics as shown to be important for the ranges of MTT and scaling relations in this work and in *Hale and McDonnell* [2016].

Acknowledgments

The authors thank the National Council for Air and Stream Improvement and the AGU Horton Research Grant for support of this work. The CUAHSI Pathfinder grant program provided opportunity for Cody Hale to receive valuable feedback from the University of Aberdeen's Northern Rivers Institute team, led by Doerthe Tetzlaff and Chris Soulsby. Markus Hrachowitz, Christian Birkel, and Rene Capell are also thanked for their valuable feedback. Tina Garland is thanked for field assistance and isotope analysis assistance. Jakob Garvelmann from the Univeristy of Freiburg is thanked for his field efforts. Two anonymous reviewers are thanked for their valuable comments on an earlier draft of this manuscript. Data used for the analyses presented here will be made available upon request from the corresponding author.

References

Aeschbach-Hertig, W., P. Schlosser, M. Stute, H. J. Simpson, A. Ludin, and J. F. Clark (1998), A $^{3}H/^{3}He$ study of ground water flow in a fractured bedrock aquifer, *Ground Water*, *36*, 661–670.

Aeschbach-Hertig, W., F. Peeters, U. Beyerle, and R. Kipfer (1999), Interpretation of dissolved atmospheric noble gases in natural waters, *Water Resour Res*, *35*, 2779–2792, doi:10.1029/1999WR900130.

Ali, G. A., C. L'Heureux, A. G. Roy, M.-C. Turmel, and F. Courchesne (2011), Linking spatial patterns of perched groundwater storage and stormflow generation processes in a headwater forested catchment, *Hydrol. Processes*, *25*, 3843–3857.

Amoozegar, A. (1989), A compact constant-head permeameter for measuring hydraulic conductivity of the vadose zone, *Soil Sci. Soc. Am. J.*, *53*, 1356–1361.

Anderson, S. P., W. E. Dietrich, R. Torres, D. R. Montgomery, and K. Loague (1997a), Concentration-discharge relationships in runoff from a steep, unchanneled catchment, *Water Resour. Res.*, *33*, 211–225, doi:10.1029/96WR02715.

Anderson, S. P., W. E. Dietrich, D. R. Montgomery, R. Torres, M. E. Conrad, and K. Loague (1997b), Subsurface flow paths in a steep, unchanneled catchment, *Water Resour. Res.*, *33*, 2637–2653, doi:10.1029/97WR02595.

Asano, Y., and T. Uchida (2012), Flow path depth is the main controller of mean base flow transit times in a mountainous catchment, *Water Resour. Res.*, *48*, W03512, doi:10.1029/2011WR010906.

Asano, Y., T. Uchida, and N. Ohte (2002), Residence times and flow paths of water in steep unchannelled catchments, Tanakami, Japan, *J. Hydrol.*, *261*(1-4), 173–192.

Benettin, P., Y. van der Velde, S. E. A. T. M. van der Zee, A. Rinaldo, and G. Botter (2013), Chloride circulation in a lowland catchment and the formulation of transport by travel time distributions, *Water Resour. Res.*, *49*, 4619–4632, doi:10.1002/wrcr.20309.

Birkel, C., C. Soulsby, and D. Tetzlaff (2011a), Modelling catchment-scale water storage dynamics: Reconciling dynamic storage with tracer-inferred passive storage, *Hydrol. Processes*, *25*, 3924–3936.

Birkel, C., D. Tetzlaff, S. M. Dunn, and C. Soulsby (2011b), Using time domain and geographic source tracers to conceptualize streamflow generation processes in lumped rainfall-runoff models, *Water Resour. Res.*, *47*, W02515, doi:10.1029/2010WR009547.

Birkel, C., C. Soulsby, and D. Tetzlaff (2014), Conceptual modelling to assess how the interplay of hydrological connectivity, catchment storage and tracer dynamics controls non-stationary water age estimates, *Hydrol. Processes*, doi:10.1002/hyp.10414.

Blumstock, M., D. Tetzlaff, I. A. Malcolm, G. Nuetzmann, and C. Soulsby (2015), Baseflow dynamics: Multi-tracer surveys to assess variable groundwater contributions to montane streams under low flows, *J. Hydrol.*, *527*, 1021–1033, doi:10.1016/j.jhydrol.2015.05.019.

Bolin, B., and H. Rodhe (1973), A note on the concepts of age distribution and transit time in natural reservoirs, *Tellus*, *25*(1), 58–62.

Bonell, M. (1993), Progress in the understanding of runoff generation dynamics in forests, *J. Hydrol.*, *150*, 217–275.

Bonell, M., and L. A. Bruijnzeel (Eds.) (2004), *Forests, Water and People in the Humid Tropics: Past, Present and Future Hydrological Research for Integrated Land and Water Management*, Cambridge Univ. Press, Cambridge, U. K.

Botter, G. (2012), Catchment mixing processes and travel time distributions, *Water Resour. Res.*, *48*, W05545, doi:10.1029/2011WR011160.

Botter, G., A. Porporato, I. Rodriguez-Iturbe, and A. Rinaldo (2009), Nonlinear storage-discharge relations and catchment streamflow regimes, *Water Resour. Res.*, *45*, W10427, doi:10.1029/2008WR007658.

Botter, G., E. Bertuzzo, and A. Rinaldo (2010), Transport in the hydrologic response: Travel time distributions, soil moisture dynamics, and the old water paradox, *Water Resour. Res.*, *46*, W03514, doi:10.1029/2009WR008371.

Botter, G., E. Bertuzzo, and A. Rinaldo (2012), Catchment residence and travel time distributions: The master equation, *Geophys. Res. Lett.*, *38*, L11403, doi:10.1029/2011GL047666.

Broxton, P. D., P. A. Troch, and S. W. Lyon (2009), On the role of aspect to quantify water transit times in small mountainous catchments, *Water Resour. Res.*, *45*, W08427, doi:10.1029/2008WR007438.
Brutsaert, W., and J. L. Nieber (1977), Regionalized drought flow hydrographs from a mature glaciated plateau, *Water Resour. Res.*, *13*, 637–644.
Cook, P. G., D. K. Solomon, W. E. Sanford, E. Busenberg, L. N. Plummer, and R. J. Poreda (1996), Inferring shallow groundwater flow in saprolite and fractured rock using environmental tracers, *Water Resour. Res.*, *32*(6), 1501–1509, doi:10.1029/96WR00354.
Cook, P. G., A. J. Love, N. I. Robinson, and C. T. Simmons (2005), Groundwater ages in fractured rock aquifers, *J. Hydrol.*, *308*, 284–301.
Corliss, J. F. (1973), Soil Survey, Alsea Area, Oregon, 82 pp., U.S. *Dep. of Agric., Soil Conserv. Serv.*, Washington, D. C.
Duvert, C., M. K. Stewart, D. I. Cendón, and M. Raiber (2016), Time-series of tritium, stable isotopes and chloride reveal short-term variations in groundwater contribution to a stream, *Hydrol. Earth Syst. Science.*, *20*, 257–277, doi:10.5194/hess-20-257-2016.
Fenicia, F., S. Wrede, D. Kavetski, L. Pfister, L. Hoffmann, H. H. G. Savenije, and J. J. McDonnell (2010), Assessing the impact of mixing assumptions on the estimation of streamwater mean residence time, *Hydrol. Processes*, *24*(12), 1730–1741.
Freeze, R. A., and J. A. Cherry (1979), *Groundwater*, 1st ed., 604 pp., Prentice Hall, Englewood Cliffs, N. J.
Frisbee, M. D., F. M. Phillips, A. R. Campbell, F. Liu, and S. A. Sanchez (2011), Streamflow generation in a large, alpine watershed in the southern Rocky Mountains of Colorado: Is streamflow generation simply the aggregation of hillslope runoff responses?, *Water Resour. Res.*, *47*, W06512, doi:10.1029/2010WR009391.
Frisbee, M. D., J. L. Wilson, J. D. Gomez-Velez, F. M. Phillips, and A. R. Campbell (2013), Are we missing the tail (and the tale) of residence time distributions in watersheds?, *Geophys. Res. Lett.*, *40*, 4633–4637, doi:10.1002/grl.50895.
Gabrielli, C. P., and J. J. McDonnell (2011), An inexpensive and portable drill rig for bedrock groundwater studies in headwater catchments, *Hydrol. Processes*, *26*, 622–632.
Gardner, P., and D. K. Solomon (2009), An advanced passive diffusion sampler for the determination of dissolved gas concentrations, *Water Resour. Res.*, *45*, W06423, doi:10.1029/2008WR007399.
Graham, C. B., and J. J. McDonnell (2010), Hillslope threshold response to rainfall: (2) Development and use of a macroscale model, *J. Hydrol.*, *393*(1-2), 77–93.
Hale, V. C., and J. J. McDonnell (2016), Effect of bedrock permeability on stream base flow mean transit time scaling relations: 1. A multiscale catchment intercomparison, *Water Resour. Res.*, *52*, doi:10.1002/2014WR016124.
Hammermeister, D. P., G. F. Kling, and J. A. Vomocil (1982), Perched watertables on hillsides in Western Oregon: I. Some factors affecting their development and longevity, *Soil Sci. Soc. Am. J.*, *46*, 811–818.
Haria, A. H., and P. Shand (2004), Evidence for deep subsurface flow routing in a forested upland Wales: Implications for contaminant transport and stream flow generation, *Hydrol. Earth Syst. Sci.*, *8*(2), 334–344.
Harman, C. J. (2015), Time-variable transit time distributions and transport: Theory and application to storage-dependent transport of chloride in a watershed, *Water Resour. Res.*, *51*, 1–30, doi:10.1002/2014WR015707.
Harr, R. D. (1976), Hydrology of small forest stream in western Oregon, *Gen. Tech. Rep. PNW-55*, 15 pp., Pac. Northwest For. and Range Exp. Stn., USDA For. Serv., Portland, Oreg.
Harr, R. D. (1977), Water flux in soil and subsoil on a steep forested slope, *J. Hydrol.*, *33*, 37–58.
Harris, D. D. (1977), Hydrologic changes after logging in two small Oregon coastal watersheds, *U.S. Geol. Surv. Water Supply Pap., 2037*.
Heidbüchel, I., P. A. Troch, S. W. Lyon, and M. Weiler (2012), The master transit time distribution of variable flow systems, *Water Resour. Res.*, *48*, W06520, doi:10.1029/2011WR011293.
Heidbüchel, I., P. A. Troch, and S. W. Lyon (2013), Separating physical and meteorological controls of variable transit times in zero-order catchments, *Water Resour. Res.*, *49*, 7644–7657, doi:10.1002/2012WR013149.
Hewlett, J. D., and A. R. Hibbert (1967), Factors affecting the response of small watersheds to precipitation in humid areas, in *Forest Hydrology*, edited by W. E. Sopper and H. W. Lull, pp. 275–291, Pergamon Press, N. Y.
Hrachowitz, M., C. Soulsby, D. Tetzlaff, J. J. C. Dawson, and I. A. Malcolm (2009), Regionalization of transit time estimates in montane catchments by integrating landscape controls, *Water Resour. Res.*, *45*, W05421, doi:10.1029/2008WR007496.
Hrachowitz, M., C. Soulsby, D. Tetzlaff, I. A. Malcolm, and G. Schoups (2010), Gamma distribution models for transit time estimation in catchments: Physical interpretation of parameters and implications for time-variant transit time assessment, *Water Resour. Res.*, *46*, W10536, doi:10.1029/2010WR009148.
Hrachowitz, M., H. Savenije, T. A. Bogaard, D. Tetzlaff, and C. Soulsby (2013), What can flux tracking teach us about water age distribution patterns and their temporal dynamics?, *Hydrol. Earth Syst. Sci.*, *17*, 533–564, doi:10.5194/hess-17-533-2013.
IAEA (2013), *Isotope Methods for Dating Old Groundwater*, Vienna.
Katsuyama, M., M. Tani, and S. Nishimoto (2010), Connection between streamwater mean residence time and bedrock groundwater recharge/discharge dynamics in weathered granite catchments, *Hydrol. Processes*, *24*(16), 2287–2299.
Kirchner, J. W. (2009), Catchments as simple dynamical systems: Catchment characterization, rainfall-runoff modeling, and doing hydrology backward, *Water Resour. Res.*, *45*, W02429, doi:10.1029/2008WR006912.
Kirchner, J. W., X. Feng, and C. Neal (2000), Fractal stream chemistry and its implications for contaminant transport in catchments, *Nature*, *403*(6769), 524–527.
Kosugi, K. I., S. Y. Katsura, M. Katsuyama, and M. Takahisa (2006), Water flow processes in weathered granitic bedrock and their effects on runoff generation in a small headwater catchment, *Water Resour. Res.*, *42*, W02414, doi:10.1029/2005WR004275.
Kosugi, K. I., M. Fujimoto, S. Y. Katsura, H. Kato, Y. Sando, and T. Mizuyama (2011), Localized bedrock aquifer distribution explains discharge from a headwater catchment, *Water Resour. Res.*, *47*, W07530, doi:10.1029/2010WR009884.
Maloszewski, P., and A. Zuber (1982), Determining the turnover time of groundwater systems with the aid of environmental tracers: 1. *Models and their applicability, J. Hydrol.*, *57*, 207–231.
Maloszewski, P., W. Rauert, W. Stichler, and A. Hermann (1983), Application of flow models in an alpine catchment area using tritium and deuterium data, *J. Hydrol.*, *66*, 319–330.
Manning, A. H., and J. S. Caine (2007), Groundwater noble gas, age, and temperature signatures in an Alpine watershed: Valuable tools in conceptual model development, *Water Resour. Res.*, *43*, W04404, doi:10.1029/2006WR005349.
Manning, A. H., J. F. Clark, S. H. Diaz, L. K. Rademacher, S. Earman, and L. N. Plummer (2012), Evolution of groundwater age in a mountain watershed over a period of thirteen years, *J. Hydrol.*, *460-461*, 13–28.
Manning, A. H., P. L. Verplanck, J. S. Caine, and A. S. Todd (2013), Links between climate change, water-table depth, and water chemistry in a mineralized mountain watershed, *Appl. Geochem.*,*37*, 64–78, doi:10.1016/japgeochem.2013.07.002.
McDonnell, J. J. (2013), Are all runoff processes the same?, *Hydrol. Processes*, *27*, 4103–4111, doi:10.1002/hyp.10076.
McDonnell, J. J., and R. Woods (2004), On the need for catchment classification, *J. Hydrol.*, *299*(1-2), 2–3.

McGuire, K. J., and J. J. McDonnell (2010), Hydrological connectivity of hillslopes and streams: Characteristic time scales and nonlinearities, *Water Resour. Res.*, *46*, W10543, doi:10.1029/2010WR009341.
McGuire, K. J., J. J. McDonnell, M. Weiler, C. Kendall, B. L. McGlynn, J. M. Welker, and J. Seibert (2005), The role of topography on catchment-scale water residence time, *Water Resour. Res.*, *41*, W05002, doi:10.1029/2004WR003657.
McNamara, J. P., D. Tetzlaff, K. Bishop, C. Soulsby, M. Seyfried, N. E. Peters, B. T. Aulenbach, and R. Hooper (2011), Storage as a metric of catchment comparison, *Hydrol. Processes*, *25*, 3364–3371.
Millares, A., M. J. Polo, and M. A. Losada (2009), The hydrological response of baseflow in fractured mountain areas, *Hydrol. Earth Syst. Sci.*, *13*(7), 1261–1271.
Monteith, D. T. (1965), Evaporation and the environment, *Symp. Soc. Exp. Biol.*, *19*, 205–234.
Montgomery, D. R., and W. E. Dietrich (2002), Runoff generation in a steep, soil-mantled landscape, *Water Resour. Res.*, *38*(9), 1168, doi:10.1029/2001WR000822.
Montgomery, D. R., W. E. Dietrich, R. Torres, S. P. Anderson, J. T. Heffner, and K. Loague (1997), Hydrologic response of a steep, unchanneled valley to natural and applied rainfall, *Water Resour. Res.*, *33*, 91–109.
Montgomery, D. R., W. E. Dietrich, and J. T. Heffner (2002), Piezometric response in shallow bedrock at CB1: Implications for runoff generation and landsliding, *Water Resour. Res.*, *38*(12), 1274, doi:10.1029/2002WR001429.
Morgenstern, U., and C. B. Taylor (2009), Ultra low-level tritium measurement using electrolytic enrichment and LSC, *Isotopes Environ. Health Stud.*, *45*(2), 96–117.
Morgenstern, U., M. Stewart, and R. Stenger (2010), Dating of streamwater using tritium in a post nuclear bomb pulse world: Continuous variation of mean transit time with streamflow, *Hydrol. Earth Syst. Sci.*, *14*, 2289–2301.
Niemi, A. J. (1978), Residence time distribution of variable flow processes, *Int. J. Appl. Radiat. Isotopes*, *28*, 855–860.
Oswald, C. J., M. C. Richardson, and B. A. Branfireun (2011), Water storage dynamics and runoff response of a boreal Shield headwater catchment, *Hydrol. Processes*, *25*(19), 3042–3060.
Personius, S. F. (1995), Late Quaternary stream incision and uplift in the forearc of the Cascadia subduction zone, western Oregon, *J. Geophys. Res.*, *100*(B10), 20193–20210, doi:10.1029/95JB01684.
Rademacher, L. K., J. F. Clark, D. W. Clow, and G. B. Hudson (2005), Old groundwater influence on stream hydrochemistry and catchment response times in a small Sierra Nevada catchment: Sagehen Creek, California, *Water Resour. Res.*, *41*, W02004, doi:10.1029/2003WR002805.
Rasmussen, T. C. (2001), Pressure wave vs. tracer velocities through unsaturated fractured rock, in *Flow and Transport Through Unsaturated Fractured Rock: An Overview*, vol. 42, pp. 45–52, AGU, Washington, D. C.
Reager, J. T., and J. S. Famiglietti (2009), Global terrestrial water storage capacity and flood potential using GRACE, *Geophys. Res. Lett.*, *36*, L23402, doi:10.1029/2009GL040826.
Rinaldo, A., K. J. Beven, E. Bertuzzo, L. Nicotina, J. Davies, A. Fiori, D. Russo, and G. Botter (2011), Catchment travel time distributions and water flow in soils, *Water Resour. Res.*, *47*, W07537, doi:10.1029/2011WR010478.
Rinaldo, A., P. Benettin, C. J. Harman, M. Hrachowitz, K. J. McGuire, Y. van der Velde, E. Bertuzzo, and G. Botter (2015), Storage selection functions: A coherent framework for quantifying how catchments store and release water and solutes, *Water Resour. Res.*, *51*, 4840–4847, doi:10.1002/2015WR017273.
Robinson, D. A., et al. (2008), Advancing process-based watershed hydrological research using near-surface geophysics: A vision for, and review of, electrical and magnetic geophysical methods, *Hydrol. Processes*, *22*(18), 3604–3635.
Rodgers, P., C. Soulsby, and D. Tetzlaff (2005), Using stable isotope tracers to assess hydrological flow paths, residence times and landscape influences in a nested mesoscale catchment, *Hydrol. Earth Syst. Sci.*, *9*, 139–155.
Roering, J. J., J. W. Kirchner, and W. E. Dietrich (2005), Characterizing structural and lithologic controls on deep-seated landsliding: Implications for topographic relief and landscape evolution in the Oregon Coast Range, USA, *Geol. Soc. Am. Bull.*, *117*(5-6), 654–668.
Sayama, T., and J. J. McDonnell (2009), A new time-space accounting scheme to predict stream water residence time and hydrograph source components at the watershed scale, *Water Resour. Res.*, *45*, W07401, doi:10.1029/2008WR007549.
Sayama, T., J. J. McDonnell, A. Dhakal, and K. Sullivan (2011), How much water can a watershed store?, *Hydrol. Processes*, *25*, 3899–3908.
Schlosser, P., M. Stute, H. Dorr, C. Sonntag, and K. O. Munnich (1988), Tritium He-3 dating of shallow groundwater, *Earth Planet. Sci. Lett.*, *89*(3-4), 353–362.
Sidle, R. C., S. Noguchi, Y. Tsuboyama, and K. Laursen (2001), A conceptual model of preferential flow systems in forested hillslopes: Evidence of self-organization, *Hydrol. Processes*, *15*, 1675–1692.
Snavely, P. D., H. C. Wagner, and N. S. MacLeod (1964), Rythmic-bedded eugeosynclinal deposits of the Tyee Formation, Oregon Coast Range, *Kans. Geol. Surv. Bull.*, *169*, 461–480.
Solomon, D. K., and P. G. Cook (2000), ^{3}H and ^{3}He, in *Environmental Tracers in Subsurface Hydrology*, edited by P. Cook and A. L. Herczeg, pp. 397–424, Kluwer Acad., Boston, Mass.
Solomon, D. K., D. P. Genereux, L. N. Plummer, and E. Busenberg (2010), Testing mixing models of old and young groundwater in a tropical lowland rain forest with environmental tracers, *Water Resour. Res.*, *46*, W04518, doi:10.1029/2009WR008341.
Soulsby, C., D. Tetzlaff, N. van den Bedem, I. A. Malcolm, P. J. Bacon, and A. F. Youngson (2007), Inferring groundwater influences on surface water in montane catchments from hydrochemical surveys of springs and streamwaters, *J. Hydrol.*, *333*(2-4), 199–213.
Soulsby, C., D. Tetzlaff, S. M. Dunn, and S. Waldron (2006), Scaling up and out in runoff process understanding: Insights from nested experimental catchment studies, *Hydrol. Process.*, *20*, 2461–2465, doi:10.1002/hyp.6338.
Soulsby, C., D. Tetzlaff, and M. Hrachowitz (2009), Tracers and transit times: Windows for viewing catchment scale storage?, *Hydrol. Processes*, *23*(24), 3503–3507.
Soulsby, C., K. Piegat, J. Siebert, and D. Tetzlaff (2011), Catchment-scale estimates of flow path partitioning and water storage based on transit time and runoff modelling, *Hydrol. Processes*, *25*, 3960–3976, doi:10.1002/hyp.8324.
Soulsby, C., C. Birkel, J. Geris, J. Dick, C. Tunaley, and D. Tetzlaff (2015), Stream water age distributions controlled by storage dynamics and nonlinear hydrologic connectivity: Modeling with high-resolution isotope data, *Water Resour. Res.*, *51*, 7759–7776, doi:10.1002/2015WR017888.
Spence, C. (2010), A paradigm shift in hydrology: Storage thresholds across scales influence catchment runoff generation, *Geogr. Compass*, *4*(7), 819–833.
Stewart, M. K., and J. T. Thomas (2008), A conceptual model of flow to the Waikoropupu Springs, NW Nelson, New Zealand, based on hydrometric and tracer (^{18}O, Cl, ^{3}H, and CFC) evidence, *Hydrol. Earth Syst. Sci.*, *12*, 1–19.
Stewart, M. K., J. Mehlhorn, and S. Elliott (2007), Hydrometric and natural tracer (^{18}O, silica, ^{3}H, and SF_6) evidence for a dominant groundwater contribution to Pukemanga Stream, New Zealand, *Hydrol. Processes*, *21*(24), 3340–3356.

Stewart, M. K., U. Morgenstern, and J. J. McDonnell (2010), Truncation of stream residence time: How the use of stable isotopes has skewed our concept of streamwater age and origin, *Hydrol. Processes*, *24*(12), 1646–1659.
Stewart, M. K., U. Morgenstern, J. J. McDonnell, and L. Pfister (2012), The 'hidden streamflow' challenge in catchment hydrology: A call to action for streamwater transit time analysis, *Hydrol. Processes*, *26*(13), 2061–2066, doi:10.1002/hyp.9262.
Swanson, F. J., and M. E. James (1975), Geology and geomorphology of the H.J. Andrews Experimental Forest, western Cascades, Oregon, *Rep. Res. Pap. PNW-188*, 14 pp., U.S. Dep. of Agric., For. Serv., Pac. Northwest For. and Range Exp. Stn., Portland, Oreg.
Tetzlaff, D., J. Seibert, K. J. McGuire, H. Laudon, D. A. Burns, S. M. Dunn, and C. Soulsby (2009), How does landscape structure influence catchment transit time across different geomorphic provinces?, *Hydrol. Processes*, *23*(6), 945–953.
Tetzlaff, D., C. Birkel, J. Dick, J. Geris, and C. Soulsby (2014), Storage dynamics in hydropedological units control hillslope connectivity, run-off generation, and the evolution of catchment transit time distributions, *Water Resour. Res.*, *50*, 969–985, doi:10.1002/2013WR014147.
Thorson, T. D., S. A. Bryce, D. A. Lammers, A. J. Woods, J. M. Omernik, J. Kagan, D. E. Pater, and J. A. Comstock (2003), *Ecoregions of Oregon*, U.S. Geol. Surv., Reston, Va.
Torres, R., W. E. Dietrich, D. R. Montgomery, S. P. Anderson, and K. Loague (1998), Unsaturated zone processes and the hydrologic response of a steep, unchanneled catchment, *Water Resour. Res.*, *34*(8), 1865–1879, doi:10.1029/98WR01140.
Uchida, T., J. J. McDonnell, and Y. Asano (2006), Functional intercomparison of hillslopes and small catchments by examining water source, flowpath and mean residence time, *J. Hydrol.*, *327*, 627–642.
Uhlenbrook S., M. Frey, C. Liebundgut, and P Maloszewski (2002), Hydrograph separations in a mesoscale mountainous basin at event and seasonal timescales, *Water Resour. Res.*, *38*(6), doi:10.1029/2001WR000938.
van der Velde, Y., I. Heidbüchel, S. W. Lyon, L. Nyberg, A. Rodhe, K. Bishop, and P. A. Troch (2014), Consequences of mixing assumptions for time-variable travel time distributions, *Hydrol. Processes*, *29*, 3460–3474, doi:10.1002/hyp.10372.
Wagener, T., M. Sivapalan, P. Troch, and R. Woods (2007), Catchment classification and hydrologic similarity, *Geogr. Compass*, *1*, 901–931.
Western, A. W., R. B. Grayson, and G. Bloschl (2002), Scaling of soil moisture: A hydrologic perspective, *Annu. Rev. Earth Planet. Sci.*, *30*, 149–180.
Weyman, D. R. (1973), Measurements of the downslope flow of water in a soil, *J. Hydrol.*, *20*, 267–288.
Whipkey, R. Z. (1965), Subsurface storm flow from forested slopes, *Bull. Int. Assoc. Sci. Hydrol.*, 2, 74–85.
Wilson, C. J., and W. E. Dietrich (1987), The contribution of bedrock groundwater flow to storm runoff and high pore pressure development in hollows, *IAHS Publ.*, *165*, 49–59.
Wondzell, S. M. (2006), Effect of morphology and discharge on hyporheic exchange flows in two small streams in the Cascade Mountains of Oregon, USA, *Hydrol. Processes*, *20*(2), 267–287.
Yee, C. S., and R. D. Harr (1977), Influence of soil aggregation on slope stability in the Oregon Coast Ranges, *Environ. Geol.*, *1*, 367–377.